

UC Irvine

UC Irvine Previously Published Works

Title

Regulatory T-cell Depletion Alters the Tumor Microenvironment and Accelerates Pancreatic Carcinogenesis

Permalink

<https://escholarship.org/uc/item/2759w6t9>

Journal

Cancer Discovery, 10(3)

ISSN

2159-8274

Authors

Zhang, Yaqing
Lazarus, Jenny
Steele, Nina G
[et al.](#)

Publication Date

2020-03-01

DOI

10.1158/2159-8290.cd-19-0958

Peer reviewed



Published in final edited form as:

Cancer Discov. 2020 March ; 10(3): 422–439. doi:10.1158/2159-8290.CD-19-0958.

Regulatory T cell depletion alters the tumor microenvironment and accelerates pancreatic carcinogenesis.

Yaqing Zhang^{1,2,*}, Jenny Lazarus¹, Nina G. Steele³, Wei Yan¹, Ho-Joon Lee⁴, Zeribe C. Nwosu⁴, Christopher J. Halbrook⁴, Rosa E. Menjivar⁵, Samantha B. Kemp⁶, Veerin R. Sirihorachai⁷, Ashley Velez-Delgado³, Katelyn Donahue⁷, Eileen S. Carpenter⁸, Kristee L. Brown¹, Valerie Irizarry-Negron¹, Anna C. Nevison¹, Alekya Vinta⁹, Michelle A. Anderson⁸, Howard C. Crawford^{2,4,8}, Costas A. Lyssiotis^{2,4,8}, Timothy L. Frankel¹, Filip Bednar^{1,*}, Marina Pasca di Magliano^{1,2,3,5,*}

¹Department of Surgery, University of Michigan, Ann Arbor, MI 48109, USA.

²Rogel Cancer Center, University of Michigan, Ann Arbor, MI 48109, USA.

³Department of Cell and Developmental Biology, University of Michigan, Ann Arbor, MI 48109, USA.

⁴Department of Molecular and Integrative Physiology, University of Michigan, Ann Arbor, MI 48109, USA.

⁵Program in Cellular and Molecular Biology, University of Michigan, Ann Arbor, MI 48109, USA.

⁶Molecular and Cellular Pathology Graduate Program, University of Michigan, Ann Arbor, MI 48109, USA.

⁷Cancer Biology Program, University of Michigan, Ann Arbor, MI 48109, USA.

⁸Department of Internal Medicine, Division of Gastroenterology, University of Michigan, Ann Arbor MI 48109, USA.

⁹College of Literature, Science, and the Arts, University of Michigan, Ann Arbor, MI 48109, USA.

Abstract

Regulatory T cells (Tregs) are abundant in human and mouse pancreatic cancer. To understand the contribution to the immunosuppressive microenvironment, we depleted Tregs in a mouse model of pancreatic cancer. Contrary to our expectations, Treg depletion failed to relieve immunosuppression, and led to accelerated tumor progression. We show that Tregs are a key

*Corresponding authors. Marina Pasca di Magliano (MPdM), marinapa@umich.edu, Mail: Rogel Cancer Center Rm. 6306, 1500 E Medical Center Dr. Ann Arbor, MI 48109, Tel: 734 936 9083, Filip Bednar (FB), filipb@umich.edu, Mail: Rogel Cancer Center Rm. 6217, 1500 E Medical Center Dr. Ann Arbor, MI 48109, Tel: 734 936 7607, Yaqing Zhang (YZ), yaqingzh@umich.edu, Mail: Rogel Cancer Center Rm. 6110, 1500 E Medical Center Dr. Ann Arbor, MI 48109, Tel: 734 763 3950.

Author contributions: MPdM directed the study. MPdM and YZ developed the study concept and were responsible for study design. FB conceived and implemented the CyTOF analysis and statistical pipeline. JL stained and analyzed and TLF coordinated the multiplex immunohistochemistry. CJH performed the in vitro macrophage polarization experiments and CAL coordinated and directed them. NS, ESC, VS, KD and MAA procured human tissue, processed for CyTOF and single cell sequencing and analyzed the data. YZ, NS, HJL, WY, ZCN, RM, SBK, AVD, KLB, VIN, ACN, AV and FB performed experiments, acquired and analyzed data. HCC helped design experiments. YZ and MPdM wrote the manuscript, which was then edited by all the co-authors. All the co-authors approved the final version of the manuscript prior to submission.

Competing interests: The authors declare no competing interests.

source of TGF β ligands and, accordingly, their depletion reprogrammed the fibroblast population, with loss of tumor-restraining, smooth muscle actin-expressing fibroblasts (myCAFs). Conversely, we observed an increase in chemokines *Ccl3*, *Ccl6*, and *Ccl8* leading to increased myeloid cell recruitment, restoration of immune suppression and promotion of carcinogenesis, an effect that was inhibited by blockade of the common CCL3/6/8 receptor CCR1. Further, Treg depletion unleashed pathological CD4⁺ T cell responses. Our data points to new mechanisms regulating fibroblast differentiation in pancreatic cancer and supports the notion that fibroblasts are a heterogeneous population with different and opposing functions in pancreatic carcinogenesis.

Keywords

Pancreatic Cancer; Pancreatic Intraepithelial Neoplasia; Regulatory T cells; Immunosuppression; Fibroblast; Myeloid cell; Tumor Associated Macrophage; C-C motif Chemokine Ligands; C-C Motif Chemokine Receptor 1; CyTOF

Introduction

Pancreatic ductal adenocarcinoma (PDA) is one of the deadliest human malignancies with a 5-year overall survival rate of ~9% (1). PDA and its most common precursor lesions, Pancreatic Intraepithelial Neoplasia (PanIN), are characterized by an extensively fibrotic microenvironment, which includes abundant infiltrating immune cells. Success in targeting the pancreatic cancer microenvironment has been inconsistent, and immunotherapy approaches such as immune checkpoint inhibition have largely failed (2,3).

Oncogenic mutations are prevalent in pancreatic cancer (4–6) and are present with high frequency in precursor lesions (7). Mouse models genetically engineered to express oncogenic Kras in the pancreas –known as KC mice– develop PanIN lesions that progress to invasive cancer over time (8,9). The formation of PanIN is accompanied by infiltration of suppressive immune cells (10), while cytotoxic CD8⁺ T cells are rare. Among these, myeloid cells are present in high abundance in the microenvironment, including both macrophages and myeloid derived suppressor cells/immature myeloid cells (10–16).

This immune suppression is functionally important, as activation of a CD8⁺ T cell mediated immune response is sufficient to block the onset of carcinogenesis (17–19) or induce tumor regression (11,18,20–22). Genetic elimination of CD4⁺ T cells results in the activation of CD8⁺ T cells and consequently prevents PanIN progression (17). Similarly, depletion of Th17 cells, a CD4⁺ T cell subset, inhibits pancreatic carcinogenesis (23). Further, analysis of long-term pancreatic cancer survivors reveal that anti-tumor T cells persist in their peripheral blood years after the initial diagnosis, further supporting the notion that activation of an anti-tumor immune response might be effective (24). However, our limited understanding of the mechanisms underlying immune suppression in pancreatic cancer limits our ability to translate these findings to the clinic.

Regulatory T cells (Tregs), defined as CD4⁺CD25⁺Foxp3⁺ T cells, accumulate in mouse and human PanIN and pancreatic cancer (10,17,25). Moreover, Treg frequency positively correlates with tumor metastasis and poor prognosis in human PDA patients (26,27).

Depletion of Tregs has been tested in a model of transplanted pancreatic cancer in mice, where it led to a CD8⁺ T-cell mediated anti-tumor immune response (21). However, the role of Tregs during the onset and progression of pancreatic cancer, as well as in spontaneous invasive tumors, had not been investigated, and is the focus of our study.

Results

Regulatory T cells are abundant in human PanIN and pancreatic cancer

To study the relative abundance of Tregs, myeloid cells and CD8⁺ T cells in human pancreatic cancer, we performed Cytometry by Time-of-Flight (CyTOF) analysis. We included 3 surgical samples from Whipple resections and 2 endoscopic ultrasound-guided core needle biopsy samples. High-dimensional analysis using FlowSOM-viSNE (28,29) revealed the presence of a CD45⁺CD3⁺CD4⁺CD25⁺ Treg population and several subsets of myeloid cells in each sample (Fig 1A and S1A) while CD8⁺ T cells were rare (Fig. 1A and S1A). To determine the localization of immune cells within the tissue, we have recently optimized the use of fluorescent multiplex immunohistochemistry system (Opal Multiplex IHC, PerkinElmer) for tumor immunophenotyping (30). Using this platform, we stained 39 human pancreatic cancer samples, 37 PanIN samples, and 52 adjacent normal or chronic pancreatitis samples –a non-cancerous inflammatory condition of the pancreas. Out of 52 chronic pancreatitis samples, only 14 had measurable Tregs (defined as CD3⁺ CD8⁻ FoxP3⁺). In contrast, Tregs were present in most of the tumor samples and often observed in close proximity of the tumor cells (Fig. 1B and S1B); their abundance positively correlated with macrophages in the same tissue (Fig. S1C) and –with two exceptions– with CD8⁺ T cells (Fig. S1C). Interestingly, Tregs were abundantly present in the PanIN samples as well, possibly indicating a role during the early stages of carcinogenesis (Fig. 1B, S1D and S1E). Similarly, in PanIN-bearing *Kras*^{+/*LSL-G12D*; *Ptf1a*^{+/*Cre*} (KC) mice (8) we observed abundant Treg infiltration by Foxp3 immunostaining (Fig. 1C). To further characterize the Treg population, we performed single cell sequencing analysis of spontaneous PanIN lesions in *iKras*^{*} mice (31), and *iKras*^{*}; *p53*^{*} (32) pancreatic cancer cells orthotopically transplanted in syngeneic mice. In both experimental systems, we detected a cell population co-expressing *Cd4*, *Cytotoxic T-lymphocyte associated protein 4 (Ctla4)*, *Foxp3* and *Interleukin-2 receptor alpha (Il2ra)*, (Fig. 1D and Fig. S1F). Similarly, in human samples (*data not shown*), *Foxp3* was co-expressed with *CTLA4* and *IL2RA*, thus in bona fide Tregs [for a review of Treg classification, see (33)],}

Treg depletion accelerated pancreatic carcinogenesis.

To study the effect of Treg depletion on the formation of PanIN, we generated *Kras*^{+/*LSL-G12D*; *Ptf1a*^{+/*Cre*; *Foxp3*^{tm3(DTR/GFP)*Ayr*} (KC;*Foxp3*^{DTR}) mice (Fig. 2A) (8,34). In these animals, Tregs can be depleted at will by administering diphtheria toxin (DT). During tissue homeostasis, Tregs play an important role in regulating the activity of the immune system and preventing autoimmune disease (34). Accordingly, depletion of Tregs for 3 weeks, starting at 4–5 weeks of age (Fig. 2B) in *Foxp3*^{DTR} mice led to systemic inflammation shown by hypertrophy of the lymphoid organs, such as increased spleen to body weight ratio (Fig. 2C, *Foxp3*^{DTR} mice). In *Foxp3*^{DTR} pancreata, Treg depletion resulted in acinar cell loss (Fig. 2D) and pancreatitis with distinct histologic changes such as acinar-ductal}}

metaplasia (ADM) –de-differentiation of acinar cells to duct-like cells (Fig. 2D, E)– and elevated immune infiltration (see immunostaining for CD45 in Fig. S2A) with characteristic presence of CD138⁺ plasma cells (Fig. S2B). In KC;Foxp3^{DTR} mice, Treg depletion led to increased spleen to body weight ratio, as well as increased pancreas to body weight ratio, a measure of tumor burden (Fig. 2C). As expected, KC pancreata had sparse lesions, consistent with their young age (Fig. 2D histopathological quantification and Fig. 2E). In contrast, Treg depletion in KC;Foxp3^{DTR} mice presented with extensive ADM and PanIN (Fig. 2D–E and S2A, PAS staining), as well as abundant immune cell infiltration (Fig. S2A).

We reasoned that the pancreatitis caused by Treg depletion synergized with oncogenic *Kras* to promote PanIN formation as shown in other experimental models of pancreatitis (35–40). We then modified the experimental design to address the role of Tregs in pre-existing PanIN. We administered Caerulein (a cholecystokinin agonist) by 8 hourly intraperitoneal injections for one day to induce acute pancreatitis in 6-week old KC and KC;Foxp3^{DTR} mice. KC;CD4^{-/-} mice were included as an additional control, as we have previously shown that lesions in CD4 ablated animals fail to progress because of productive anti-tumor immunity (17). The mice were allowed to develop PanIN lesions for 8 weeks post caerulein treatment and then received DT for 10 days or 3 weeks (Fig. 2F). The two cohorts showed a similar phenotype. Following this treatment, KC;Foxp3^{DTR} mice had increased pancreas/body ratio compared with either KC or KC;CD4^{-/-} mice (Fig. 2G). Histological analysis of the pancreata showed acinar areas with interspersed lesions in KC and KC;CD4^{-/-} mice. In contrast, KC;Foxp3^{DTR} mice had widespread lesions that almost completely replaced the pancreas parenchyma (Fig. 2H–I and S2C).

Treg depletion alters the fibroblast populations in PanIN lesions.

PanIN lesions, like pancreatic cancer, are surrounded by a fibrotic microenvironment. Accordingly, α -smooth muscle actin (SMA) staining of KC pancreata revealed characteristic areas of SMA⁺ cells surrounding the epithelial lesions (Fig. 3A and B). Intriguingly, lesions in KC;Foxp3^{DTR} pancreata lacked SMA expression, whether carcinogenesis was or was not accelerated by the induction of pancreatitis (Fig. 3A and B), while immunostaining for the fibroblast marker PDGFR β appeared unchanged (Fig. 3B). We then counted PDGFR β ⁺ cells and SMA⁺ cells in KC and KC;Foxp3^{DTR} pancreata, and calculated their ratio. The data revealed no change in total fibroblast numbers, but a reduction in SMA⁺ fibroblasts, a finding that is consistent with reprogramming of the fibroblast population (Fig. 3B). Consistent with the immunostaining data, α -SMA (*Acta2*) mRNA expression was lower in KC;Foxp3^{DTR} compared to KC pancreata. Extracellular matrix (ECM) genes such as *Collagen Type I (Col1)* and *Fibronectin 1 (Fn1)*, as well as genes related to fibroblast activation and ECM synthesis such as *Transforming growth factor β 1 (Tgf β 1)* and *Connective tissue growth factor (Ctgf)* were also down-regulated in KC;Foxp3^{DTR} compared to KC pancreata (Fig. 3C). We identified the cellular source of *Tgf β 1* and putative responsive cells expressing the *Tgf β* receptors by single-cell RNA sequencing of mouse PanIN and pancreatic cancer. *Tgf β 1* was expressed by both epithelial cells and T cells, including Tregs. Conversely, the three *Tgf β* receptors were expressed in the majority of fibroblasts, as well as a subset of epithelial cells (Fig. 3D). Supporting these findings, TCGA database (<https://www.cbioportal.org/datasets>) analysis revealed a positive correlation

between a Treg signature and expression of *ACTA2* and *TGFB* signaling genes in human tumors (Fig. S1G–I). SMA^{high} fibroblasts define the “myofibroblastic CAFs” (myCAFs) population of cancer-associated fibroblasts, a phenotype that is driven by *Tgfβ* (41,42). Our data is consistent with the notion that Tregs are a source of *Tgfβ* and drive myCAF differentiation of fibroblasts.

Immunosuppressive myeloid cells increase upon Treg depletion.

We then set out to determine the effect of Treg depletion on the immune microenvironment. To compare the immune infiltration among different groups, we devised a protocol that would result in a similar lesion load in the different genotypes, namely KC, KC;CD4^{-/-} and KC;Foxp3^{DTR}. In brief, adult mice received 8 hourly caerulein injections in a day. Eight weeks later, they were treated with DT for 1 week and then harvested for histology and flow cytometry (Fig. 4A and S2D). PanIN lesions in mice lacking CD4⁺ T-cell regress over time in a CD8⁺ T cell-mediated manner (17). Consistently, KC;CD4^{-/-} mice had increased CD8⁺ T cells and increased Interferon γ (IFN γ) expressing CD8⁺ T cells compared to KC mice (Fig. 4B). In contrast, in KC;Foxp3^{DTR} pancreata we observed only a modest increase in CD8⁺ T cells and no change in IFN γ ⁺;CD8⁺ T cells compared to KC mice. In contrast, we observed an overall increase in immune cells (CD45⁺) and an increase in CD4⁺ T cells, as well as the expected loss of FoxP3⁺ cells. These data indicated that little/no productive immune response was elicited, notwithstanding the depletion of Tregs. By flow cytometry, total myeloid cells (CD11b⁺) and macrophages (CD11b⁺F4/80⁺) (% of total cells) trended towards an increase, while immature myeloid cells/myeloid-derived suppressor cells (MDSCs) (CD11b⁺Ly6C⁺Ly6G⁺F4/80⁻) were elevated in KC;Foxp3^{DTR} and KC;CD4^{-/-} pancreata compared to KC (Fig. 4C). Immunostaining of KC and KC;Foxp3^{DTR} pancreas tissue showed an increase in CD8⁺ T cells in proximity of the lesions, but we also observed a comparable increase in F4/80⁺ macrophages in those areas (Fig. S2E). Myeloid cells have a known immune suppressive function (11,13,18), thus we hypothesized that an increase in their number or suppressive potential might explain the difference in phenotype between Treg depletion and CD4 elimination during pancreatic carcinogenesis.

To assess the changes in the myeloid compartment upon Treg depletion, we performed a comparative transcriptomic analysis of the myeloid cells (DAPI⁻EpCAM⁻CD45⁺CD11b⁺) sorted from KC and KC;Foxp3^{DTR} tumors (Fig. 4D). The RNAseq results, including Principal Component Analysis (PCA) plot and a volcano plot, illustrating differential gene expression in myeloid cells are shown in Fig. S3A and B. Interestingly, we detected an increase in *Arg1*, *Chi3l3* (also known as *Ym1*), *Retnla* and *Programmed cell death 1 ligand 2* (*Pdcd1lg2*) expression in myeloid cells derived from KC;Foxp3^{DTR} pancreata, while *Interleukin-1 (III) β* was down-regulated (Fig. 4E). Further, we observed an increase in Arginase1 and Chil3l3 expression –markers of tumor associated macrophages (TAM) with immunosuppressive function (43,44)– in both fibroblasts and macrophages (Fig. S2E). By flow cytometry, we observed that cell surface Programmed death-ligand 1 (PD-L1) protein expression was elevated in TAMs (CD45⁺CD11b⁺F4/80⁺), epithelial cells (CD45⁻EpCAM⁺) and fibroblasts (CD45⁻EpCAM⁻PDGFR α ⁺) in KC;Foxp3^{DTR} compared to KC pancreata (Fig. 4F). Taken together, our data indicates that a compensatory immunosuppressive program is activated upon Treg depletion in mice bearing PanIN lesions.

The changes in expression of individual genes could be explained either by gene expression changes across the entire myeloid population, or by changes in the composition of cells types within the myeloid population. To evaluate these possibilities, we proceeded to immunophenotype our samples by CyTOF with 16 validated antibodies (Table S1). viSNE analysis suggested there were at least 11 different populations in our dataset (Fig. 5A, B and Fig. S3C) and FlowSOM analysis with supervised hierarchical clustering identified 21 separate populations (Fig. 5C). Among these, we identified multiple myeloid subpopulations, including monocytic myeloid-derived suppressor cells (Ly6C⁺), granulocytic MDSCs (Ly6G⁺), infiltrating monocytes (CD11b⁺), and macrophage/dendritic cell subsets (F4/80^{dim/+} and CD11c⁺, respectively). Interestingly, we found that both the monocyte/MDSC and macrophage subpopulations could be further divided based on the intracellular expression of arginase 1 (population 5 versus 6 and populations 15–18 versus 19–21). When we analyzed the frequency of each subpopulation in the KC versus KC;Foxp3^{DTR} mice, we found a consistent increase in the frequency of Arg1⁺ myeloid subsets after Treg depletion (Fig. S3D). By flow cytometry, we found that the percentage of CD206⁻iNOS⁺ classically activated macrophages remained unchanged, while, CD206⁺Arg1⁺ macrophages increased more than 8-fold upon Treg depletion (Fig. 5D), compared to KC control. More interestingly, we found a non-immune cell population (CD45⁻CD11b⁺)—possibly a subset of stromal fibroblasts—also expressed higher level of Arg1 in KC;Foxp3^{DTR} pancreata upon Treg depletion (Fig. 5E). Therefore, Treg depletion resulted in compensatory increase in a prevalently myeloid-driven immune suppression program.

Treg depletion results in compensatory immune suppression in late-stage disease.

Treg depletion was recently reported to induce anti-tumor immune responses and inhibit tumor growth in a transplantation model of pancreatic cancer (21). We thus reasoned that either the stage of disease (onset vs advanced disease) or different models (spontaneous vs transplanted tumors) explained the divergent findings. To investigate this apparent inconsistency, we implanted a KPC (Ptf1aCre; LSL-Kras; P53^{R172H/+}) (45) pancreatic cancer cell line (7940B) (46) orthotopically into syngeneic C57BL/6 Foxp3^{DTR} mice and depleted Tregs 11 days later (Fig. S4A). At harvest (day 20) we observed smaller tumors in the Foxp3^{DTR} cohort (Fig. S4B), and an increase in the expression of CD8⁺ T cell activation markers *Ifny*, *Granzyme B* (*Gzmb*) and *Perforin* (*Prfl*) (Fig. S4C). Consistent with activation of anti-tumor immunity, concurrent depletion of CD8⁺ T cells partially rescued tumor growth (Fig. S4B). Flow cytometry analysis revealed increased CD8⁺ T cells and myeloid cells, including macrophages, upon Treg depletion (Fig. S4D). Immunostaining confirmed increased immune infiltration and apoptosis in Treg depleted tumors (Fig. S4E). At the same time, we observed fewer SMA positive fibroblasts and more expression of immunosuppressive factors Chi313 (notably in tumor epithelial cells) and Arg1 in Foxp3^{DTR} tumors (Fig. S4E and F), which were consistent with our findings in the KC;Foxp3^{DTR} model. We then repeated a similar set of experiments in KPC;Foxp3^{DTR} (Ptf1aCre; LSL-Kras; P53^{R172H/+}; Foxp3^{DTR}) mice that develop spontaneous invasive pancreatic cancer. Upon detection of a tumor by ultrasound imaging, we administered DT to deplete Tregs (or used vehicle control) and followed tumor growth (Fig. S4G). In this setting, we observed continued tumor growth even following Treg depletion. Upon harvesting and

immunostaining, we observed both an increase in CD8⁺ T cells and an increase in myeloid cells (Fig. S4G). Our data are consistent with Treg depletion failing to elicit a productive anti-tumor immune response at late stage disease, likely due to compensatory myeloid-driven immune suppression.

Multiple CCR1 ligands are upregulated in epithelial cells and fibroblasts upon Treg depletion.

To elucidate a potential causal link between the changes in the fibroblast and epithelial compartments and the shift in immune composition upon Treg depletion, we flow sorted epithelial cells (CD45⁻EpCAM⁺) and fibroblasts (CD45⁻EpCAM⁻PDGFR α ⁺) from KC and KC;Foxp3^{DTR} pancreata (n=3 for each group) (Fig. 6A, B) and performed RNA sequencing. We then analyzed the secretome transcripts in both compartments. Interestingly, overall gene expression, as well as expression of secreted factors, showed a distinct pattern in both epithelial cells and fibroblasts upon Treg depletion (Fig. 6C and Fig. S5A, B). Among more than 400 differentially expressed secreted chemokines, cytokines and immunosuppressive factors, we observed that the *C-C motif chemokine ligands* *Ccl3*, *Ccl6*, *Ccl8*, (Fig. 6D) were among the top upregulated secreted factors in fibroblasts and/or epithelial cells upon Treg depletion, while interleukins such as *Il1 β* were downregulated but to a lesser extent compared to what we saw earlier in the myeloid cell compartment (Fig. 4E). We validated these changes by qRT-PCR in 4–8 samples/genotype (Fig. 6E and S5C). Finally, immunostaining confirmed upregulated expression of CCL8 in KC;Foxp3^{DTR} pancreata (Fig. 6F) compared to KC. Other notable changes in epithelial cells and fibroblasts were an increase in immunosuppressive factors such as *Arg1* and *Chi3l3*, as well as immune check point molecules *Cd274* (also known as *PD-L1*) and *Pdcd1lg2* (Fig. 6E and S5C).

CCL3, CCL6, and CCL8 bind a common receptor, CCR1, and they are known chemo-attractants for myeloid cells (47). We identified 4 subsets of myeloid cells in PanINs and 3 in PDA by Single-cell sequencing analysis (Fig. S1F). Myeloid 1 = MDSCs (high expression of *Itgam*, *Cd14*, *Fcgr3*, *S100a8*, *Ly6g*); myeloid 2 = macrophages (high expression of *Itgam*, *Cd68*, *Adgre1*, *Mrc1*); myeloid 3 = dendritic cells (high expression of *Itgax*, *H2-Eb1*, *Batf3*, *Itgae*, *Clec9a*) and myeloid 4 = monocytes (high expression of *Itgax*, *Ly6c2*). Of note, myeloid 4 was not detected in tumors, but only in PanIN samples. Single-cell sequencing analysis of mouse PDA or PanINs confirmed that expression of *Ccr1* was restricted to the myeloid compartment and included MDSCs and macrophages (Fig. 6G). We validated these findings *in vitro* by qRT-PCR from bone-marrow-derived macrophages (M0) polarized to M1 with lipopolysaccharide (LPS), to M2 with Interleukin-4 (IL4) and to Tumor Educated Macrophages (TEMs) with pancreatic cancer cell conditioned media. *Ccr1* expression was lowest in M1 macrophages, and highest in TEMs (Fig. 6H). Our single cell sequencing analysis also revealed that myeloid cells are the main source of *Il1a* both in PanINs and in pancreatic cancer, while the receptor *Il1r* is expressed in a subset of epithelial cells and in the vast majority of fibroblasts (Fig S5D). The expression of *Il1a* was not different in KC and KC;FoxP3^{DTR} myeloid cells, epithelial cells and fibroblasts (Fig. S5E). IL1 α drives differentiation of “inflammatory CAFs” (iCAFs), a pro-inflammatory subset of fibroblasts which also expresses elevated IL6 (41), and *Il6* was similarly unchanged in our model (*data not shown*). Thus, while fibroblasts in KC;FoxP3^{DTR} become more inflammatory at least

pertaining recruitment of myeloid cells, they might not fit exactly in the iCAF subtype, consistent with the complexity of this cell type (42,48).

CCR1 inhibition rescues Treg depletion-induced PanIN progression.

Our data to this point demonstrated that Treg depletion resulted in an increase in several CCR1 ligands, and a corresponding influx of immune-suppressive myeloid cells. To determine whether CCR1 activation is responsible for the increased myeloid infiltration and increased tumorigenesis, we utilized a commercial CCR1 inhibitor, BX471 (hereby termed CCR1i). We treated PanIN-bearing KC;Foxp3^{DTR} mice with CCR1i for a week and at the same time we depleted Tregs (Fig. 7A). At endpoint, KC;Foxp3^{DTR} mice that received DT and vehicle control showed enlarged pancreata and spleens compared to KC mice, an effect that was reversed by CCR1i treatment (Fig. S6A). Further, histopathological analysis revealed more acini and less ADM/PanIN (CK19⁺ cells) in KC;Foxp3^{DTR} mice treated with CCR1i (Fig. 7B and S6B). Immunostaining for CD45-F4/80 showed decreased total immune infiltration and macrophages (Fig. 7B and S6C), although the level of immune infiltration remained elevated compared to KC mice (*data not shown*). Thus, CCR1 inhibition bypassed Treg-depletion acceleration of carcinogenesis in KC mice driven by infiltration of immunosuppressive myeloid cells.

CD4⁺ T cells promote carcinogenesis upon Treg depletion.

Reprogramming of fibroblasts and consequent increased infiltration of myeloid cells restored immune suppression upon Treg depletion. However, we were intrigued by the increase in total CD4⁺ T cells upon Treg depletion, and by the acceleration of carcinogenesis in contrast with genetic or antibody-driven CD4⁺ T cell depletion (17,23). We thus reasoned that Tregs might normally restrain pathogenic Th2 or Th17 responses, both of which have been associated with tumor progression in pancreatic cancer (23,49). By flow cytometry, we observed an increase in CD3⁺CD8⁻CD4⁺Ifn γ ⁺ T cells in KC;Foxp3^{DTR} pancreata compared with both KC and KC;CD4^{-/-} mice (Fig. S6D). Analysis of the cytokine profile in sorted T cells from KC;Foxp3^{DTR} pancreata revealed an increase in the Th2 cytokines *Il4*, *Il10* and *Il13*, and a reduction in Th1 cytokines such as *Il2* and *Tnfa*, and well as *Il22* and *Il17* in KC;Foxp3^{DTR} mice. Our data is thus consistent with a mixed Th1/Th2 response, but the cytokine profile suggests a prevalence of a Th2 response (50) (Fig. S6E). We then depleted CD4⁺ T cells from wild type, FoxP3^{DTR}, KC and KC;Foxp3^{DTR} mice. Isotype control IgG was administered to the control cohorts and DT was administered for consistency with previous experiments, as indicated (Fig. 7C). While Treg depletion causes pancreatitis, CD4⁺ T cell depletion had no effect on wild type mice. Similarly, CD4 depletion did not accelerate carcinogenesis in young KC mice (prior to lesion formation), while Treg depletion promoted widespread metaplasia, PanIN formation and accumulation of fibroinflammatory stroma (Fig. 7D and S6F). Interestingly CD4⁺ T cell depletion prevented the formation of metaplasia and PanIN in KC;Foxp3^{DTR} mice, as well as ameliorated the pancreatitis in FoxP3^{DTR} mice (Fig. 7D). CD4⁺ T cell depletion also prevented the extensive immune infiltration and T cell infiltration elicited by Treg depletion (Fig. S6G). Together, our data point to multiple roles for Tregs within the pancreatic cancer microenvironment, that include restraining pathogenic T cell responses caused by other CD4⁺ T cell subsets.

Discussion

Pancreatic cancer precursor lesions, such as Pancreatic Intraepithelial Neoplasia, are surrounded by a fibroinflammatory stroma that persists in late-stage disease (for review see (4)). While immune cells are prevalent surrounding the lesions, they are mostly suppressive in nature (10). CD4⁺ T cells, and among those regulatory T cells, are the most abundant T cell population, while CD8⁺ T cells are rare. Depletion of CD4⁺ T cells inhibits PanIN formation (17,23); although it is insufficient to activate anti-tumor immunity at later stages (51). Treg depletion is sufficient to induce anti-tumor immunity in melanoma (52). Further, Treg depletion in orthotopically transplanted tumors derived from the KPC model (expressing both mutant Kras and p53 (45)) in syngeneic C57/Bl6 mice causes CD8⁺ T cell mediated tumor regression (21), a finding that we reproduce here. Here, we generated KC;FoxP3^{DTR} and KPC;FoxP3^{DTR} mice, where Tregs can be depleted at will in the context of spontaneous carcinogenesis. In contrast with previous findings, we show that Treg depletion in mice before or after the development of PanIN caused accelerated neoplastic progression. In invasive tumors in KPC;FoxP3^{DTR} mice, Treg depletion failed to restrain tumor growth. Analysis of the tissue revealed that an increase in CD8⁺ T cells upon Treg depletion was offset by a compensatory increase in other CD4⁺ T cells, immunosuppressive myeloid cells, and by reprogramming of the fibroblast population, from predominantly SMA expressing to largely SMA low (Fig. 7E and 7F).

The role of fibroblasts in pancreatic cancer is complex and different studies have provided contradictory results. Depletion of specific fibroblast subsets, such as the FAP⁺ cell, resulted in a reduction in tumor growth and improved response to immunotherapy (53). Conversely, depletion of SMA⁺ fibroblasts resulted in tumor promotion (54). A solution to this apparent contradiction came from the observation that heterogeneous fibroblast populations are present in the pancreatic cancer stroma (42,48). The SMA-high myCAF population is predominantly driven by TGFβ and has been described as tumor restraining (42,54). We thus measured *TGFβ* mRNA levels and found them reduced in the pancreas of Treg depleted mice. Using single cell sequencing, we determined that tumor epithelial cells, myeloid cells and T cells, including Tregs are the sources of TGFβ1 within the tissue. Conversely, epithelial cells and pancreatic fibroblasts express TGFβ receptors. TGFβ signaling in epithelial cells is known to be tumor suppressive at early stages of carcinogenesis (55); thus, a direct effect of TGFβ reduction might partially explain the increase in carcinogenesis upon Treg depletion. We also observed fibroblast reprogramming upon Treg depletion, from tumor-restricting and SMA^{high} myCAFs to a tumor-promoting fate, providing *in vivo* evidence of a phenomenon described in tumor organoids by the Tuveson laboratory (41). Conversely, we did not observe changes in *Il1a*, a key driver of iCAF differentiation (41). We show that reprogrammed fibroblasts have increased secretion of chemokines that act as chemoattractant for suppressive myeloid cells. In addition to an increase in myeloid cells, Treg depletion also resulted in elevated expression of immune suppressive genes in fibroblasts, such as *Arginase 1* and *Cd274* (PD-L1). Clinically, fibroblast reprogramming using different approaches – such as vitamin D analogs, inhibition of focal adhesion kinase – as well as remodeling of the extracellular matrix are actively being tested for pancreatic cancer therapy (56–59).

To obtain mechanistic insight into the paradoxical Treg depletion driven tumor progression, we sequenced RNA of flow sorted fibroblasts from Treg depleted KC pancreata, and uncovered increased expression in a number of chemokines, most notably *Ccl3*, *Ccl6*, *Ccl8*. CCL3 (or macrophage inflammatory protein 1-alpha, MIP-1-alpha) and CCL8 (or monocyte chemoattractant protein 2, MCP-2), are chemotactic for many different immune cells, including macrophages and other myeloid cells (47). *Ccl6* is a potent chemoattractant for macrophages and other immune cells in rodents (60). These three CCLs share a common chemokine receptor, CCR1 (47), expressed by myeloid cells and implicated in myeloid cell recruitment in rheumatoid arthritis (61) as well as myeloma and colon cancer (62,63). CCR1 inhibition reduced myeloid infiltrates and reduced PanIN progression, supporting the notion that myeloid suppressive cells are a key mediator of immune suppression in pancreatic cancer (11–13,18). Treg depletion also unleashed pathologic T cell responses that we attributed to a Th2-type response based on the cytokine profile of the tissue. Th2 cells, as well as Th17, have been implicated in the promotion of pancreatic carcinogenesis (23,49). Thus, several parallel mechanisms might explain the paradoxical promotion of carcinogenesis upon Treg depletion, and support the notion that Tregs might not be a key mediator of immune suppression of pancreatic cancer (64).

In summary, our work reveals a complex cellular cross-talk within the neoplastic pancreas that includes multiple mechanisms to induce immunosuppression. Currently, CCR2 and CXCR2 inhibition is being tested in clinical trials for pancreatic cancer, based on positive results in preclinical models (65–67). Based on our results, CCR1 blockade should be considered as an additional potential target to inhibit myeloid cell infiltration in the pancreas.

Materials and Methods

Mice

KC;Foxp3^{DTR} mice were generated by crossing KC (Ptf1a-Cre;LSL-Kras^{G12D}) (8) with Foxp3^{DTR} mice (B6.129(Cg)-Foxp3^{tm3(DTR/GFP)Ayr/J}, Jackson Laboratory) (34).

KC;CD4^{-/-} mice were generated by crossing KC with CD4-deficient mice (B6.129S6-*Cd4*^{tm1Kmw/J}, Jackson Laboratory).

Animal experiments

For Treg depletion, Foxp3^{DTR}, KC;Foxp3^{DTR} mice were treated with diphtheria toxin (DT) (50 ng/g) (Enzo Life Science) by intraperitoneal injection (i.p.). DT injections were repeated according to the specific experimental design shown in Figures. Control mice lacking Foxp3^{DTR} alleles received the same DT treatments. In KC, KC;Foxp3^{DTR} and KC;CD4^{-/-} mice, mild acute pancreatitis was induced in 4–5-week-old mice by a series of 8 hourly intraperitoneal injections of caerulein (Sigma-Aldrich, 75 µg/kg) over 1-day period. For CCR1 inhibition, mice were subcutaneously dosed with CCR1 antagonist BX471 (Sigma-Aldrich, 50 mg/kg) for 7 days at 12-hour intervals. DMSO was used as vehicle to dissolve BX471 at a concentration of 50 mg/ml.

To establish the orthotopic pancreatic cancer model, 1×10^5 of 7940B cells (C57BL/6J strain) (46) derived from KPC tumor (Ptf1a-Cre; LSL-Kras^{G12D}; p53^{flox/+}) were injected into Foxp3^{DTR} mice of compatible genetic background. Cells were tested for mycoplasma free by MycoAlert™ PLUS Mycoplasma Detection Kit (Lonza) and passage 15–20 were used for all experiments. For CD8⁺ T cell depletion, anti-CD8 mAb (BioXcell clone 2.43; 200 µg/mouse) was injected i.p. twice per week. For CD4⁺ T cell depletion, anti-CD4 mAb (BioXcell clone GK1.5; 200 µg/mouse) was injected i.p. at least every three days.

In vitro macrophage polarization

Mouse bone marrow cells were treated with L929 conditioned media for 5 days for macrophage differentiation; primary mouse pancreatic cancer cell iKras#1 (18) conditioned media was used to further educate macrophages. In addition, LPS or IL4 was used to polarize differentiated macrophages as previously described (68).

Histopathological analysis

Tissues were fixed overnight in 10% neutral-buffered formalin, embedded in paraffin and sectioned. Hematoxylin and eosin (H&E), Periodic Acid Schiff (PAS), Gomori's Trichrome, immunohistochemical and immunofluorescent staining were performed on formalin-fixed, paraffin embedded mouse pancreatic tissues as described before (17). Antibodies used are listed in Supplementary Materials Table S1. For immunofluorescence, Alexa Fluor (Invitrogen) secondary antibodies were used. Cell nuclei were counterstained with Prolong Diamond Antifade Mountant with DAPI (Invitrogen). In addition, TSA Plus Fluorescein system (PerkinElmer) was used when double immunofluorescence staining with primary antibodies raised in the same species. Images were taken using Olympus BX53F microscope, Olympus DP80 digital camera, and CellSens Standard software. The confocal images were acquired using Olympus IX-71 confocal microscope with FluoView FV500/IX software. Quantitative analysis for immunofluorescence staining was performed in at least 3 random non-overlapping fields (200× magnification) in each sample using ImageJ software to measure the percentage of positive area. To quantify the positive cell number, we used confocal images at 600× magnification. At least three samples per group were analyzed. Histopathological quantification for H&E staining was performed by a pathologist (WY) on de-identified images as previously described (69).

Opal Multiplexed IHC staining and multispectral imaging

A formalin fixed paraffin embedded tissue microarray containing human PDA, PanIN and chronic pancreatitis was acquired from the University of Michigan. Blocks were sectioned onto slides creating a 5 micron thickness per core. The slides were then processed using the Opal 7 manual kit (PerkinElmer). Images were captured on the Mantra™ Quantitative Pathology Work Station (Perkin Elmer) and analyzed using inForm® Cell Analysis™ software (Perkin Elmer), as previously described (30). For detailed methods, see Supplementary Methods (complex phenotype design for multispectral imaging analysis in Table S2).

Flow cytometry and Fluorescence-activated cell sorting (FACS)

Single-cell suspensions of pancreata were prepared and stained with fluorescently conjugated antibodies as previously described (17). Flow cytometric analysis was performed on a Cyan™ ADP analyzer (Beckman Coulter) and data were analyzed with FlowJo v10 software. FACS was performed using MoFlo Astrio (Beckman Coulter). Antibodies were listed in Supplementary Materials Table S1.

Cytometry by Time-of-Flight (CyTOF)

Single-cell suspensions of mouse pancreata were prepared as previously described (17). Human patient tissues from FNB or surgery were immediately placed into DMEM media supplemented with Y27632 (Rho-Kinase inhibitor) for transport to the laboratory. Whole blood was collected pre-operatively into 2 ten mL EDTA tubes and transported to the laboratory. Tissues were mechanically minced and enzymatically digested with collagenase P (1mg/mL DMEM) and subsequently filtered through a 40 µm mesh to obtain single cells. Up to 1×10^7 cells was stained with Cell-ID Cisplatin (1.67 µM) for 5 minutes at room temperature, and then a Combining Fix and Perm Sensitive Surface Epitopes and Nuclear Antigen Staining protocol was followed according to manufacturer's instructions (Fluidigm) for mouse samples, and as previously described (70). Analysis was performed using the Premium CytoBank Software (cytobank.org). Additional details are provided in the Supplementary Methods section.

RNA sequencing and Data analysis

Cell lysates of FACS sorted cells were homogenized using QIAshredder, then total RNA samples were isolated using RNeasy Plus Micro Kit (Qiagen), including an on-column DNase treatment using RNase-Free DNase Set (Qiagen) according to manufacturer's instruction. RNA concentration and quality were determined, and Strand mRNA libraries were prepared by the University of Michigan Sequencing Core. Libraries were sequenced using paired end 50 cycle reads on a HiSeq 4000 (Illumina). Raw data are available at the NCBI's Gene Expression Omnibus database (GSE120395 and GSE128707).

The raw data were processed and analyzed by the University of Michigan Bioinformatics Core. The quality control was done using FastQC (version v0.11.3, <http://www.bioinformatics.bbsrc.ac.uk/projects/fastqc/>) for both pre- and post-alignment and raw reads were aligned to the mouse reference genome of UCSC mm10 (<http://genome.ucsc.edu/>) using Bowtie2 (version 2.2.1) and TopHat (version 2.0.13) of the Tuxedo suite. Gene expression quantitation and differential expression analysis were performed using HTSeq (version 0.6.1) and DESeq2 (version 1.14.1). Differentially expressed genes were defined by false discovery rate (FDR) of 0.05 and fold changes of 1.5 or more. For the secretome data, we used the intersection of MetazSecKB (curated secreted) and UniProt (secreted, reviewed, <https://www.uniprot.org/>) as of 11/2017. Plots and heatmaps were generated in R/Bioconductor.

Single-cell RNA sequencing

Orthotopic pancreatic cancer model was established by injecting 5×10^4 of iKras*F1 cells (FVB/N strain) derived from iKras*;p53* tumor (Ptf1aCre;TetO-

Kras^{G12D};R26^{rtTa-IRES-EGFP};p53^{R172H/+})(32) into wild type mice of compatible genetic background. PanIN lesions were induced in iKras* (Ptf1aCre;TetO-Kras^{G12D};R26^{rtTa-IRES-EGFP}) mice by caerulein and doxycycline as previously described (31). Single-cell suspensions of pancreatic tumors were derived as previously described (17). Dead cells were removed using MACS® Dead Cell Removal Kit (Miltenyi Biotec Inc.). Single-cell cDNA library was prepared and sequenced at the University of Michigan Sequencing Core using the 10x Genomics. Samples were run using paired end 50 cycle reads on HiSeq 4000 (Illumina) to the depth of 100,000 reads.

The raw data were processed and analyzed by the University of Michigan DNA Sequencing Core. R package Seurat version 2.3.4 was used for single cell RNA-seq data analysis similarly as previous described (71). Data were initially filtered to only include all cells with at least 200 genes and all genes in greater than 3 cells. Data were initially normalized using the NormalizeData function with a scale factor of 10,000 and the LogNormalize normalization method. Variable genes were identified using the FindVariableFeatures function. Data were assigned a cell cycle score using the CellCycleScoring function and a cell cycle difference was calculated by subtracting the S phase score from the G2M score. Data were scaled, centered and batch corrected using linear regression on the counts, the cell cycle score difference and run ID using the ScaleData function. Principal Component Analysis (PCA) was run with the RunPCA function using the previously defined variable genes. Violin plots were then used to filter data according to user-defined criteria. Cell clusters were identified via the FindClusters function using a resolution of 1.2 for all samples and t-distributed Stochastic Neighbor Embedding (t-SNE) clustering algorithms were performed. FindMarkers table was created and clusters were defined by user-defined criteria. Raw data are available at the NCBI's Gene Expression Omnibus database (GSE140628).

TCGA Data Analysis

The human pancreatic adenocarcinoma RNA-Seq data from the cancer genome atlas (TCGA) was downloaded from cBioportal (<https://www.cbioportal.org/datasets>). The tumor samples were ranked based on FOXP3 expression and assigned into FOXP3 low (n=89) or FOXP3 high (n=88) groups. The differentially expressed genes between the two groups were determined using limma bioconductor package with voom function in R software (<https://www.r-project.org/>).

Quantitative RT-PCR

Total RNA samples were isolated from frozen pancreatic tissues using PureLink™ RNA Mini Kit (Invitrogen) or from cells using RNeasy Plus Micro Kit (Qiagen). High Capacity cDNA Reverse Transcription kit (Applied Biosystems) was used to reverse-transcribed total RNA into cDNA. Quantitative PCR was prepared with 1X SYBR Green PCR Master Mix (Applied Biosystems) and various primers (primer sequences are listed in Supplementary Materials Table S3). All primers were optimized for amplification under reaction conditions as follows: 95°C 10mins, followed by 40 cycles of 95°C 15 secs and 60°C 1min. Melt curve analysis was performed for all samples after the completion of the amplification protocol. Cyclophilin A was used as the housekeeping gene expression control.

Statistics

Graphpad Prism 7 software was used for all statistical analysis. All data were presented as means \pm standard error (SEM). Intergroup comparisons were performed using Two-tailed unpaired *t*-test, and $p < 0.05$ was considered statistically significant. Pearson correlation coefficients were used to measure R and R². Comparison between genotypes using the individually defined immune subpopulations was corrected for multiple comparisons with the Benjamini-Hochberg method with an FDR of 0.1.

Study approval

All animal studies were conducted in compliance with the guidelines of the Institutional Animal Care & Use Committee (IACUC) at the University of Michigan. Patient selection/sample procurement: patients over the age of 18 referred for diagnostic endoscopic ultrasound of a pancreas mass lesion suspected of PDAC were consented according to IRB HUM00041280. Up to 2 extra passes were taken for research after biopsy obtained for clinical use. Surgical specimens were obtained from patients referred for Whipple or distal pancreatectomy according to IRB HUM000025339. Written informed consent forms were obtained from the patients, and the studies were conducted in accordance with recognized ethical guidelines. Human patient studies were approved by Institutional Review Boards of the University of Michigan Medical School.

Supplementary Material

Refer to Web version on PubMed Central for supplementary material.

Acknowledgments:

We thank Dr. Gregory Beatty (University of Pennsylvania) for generously sharing the primary mouse pancreatic cancer cell line 7940B. The Ptf1a-Cre mouse was generous gift from Dr. Chris Wright (Vanderbilt University). The CK19 antibody was obtained from the Iowa Developmental Hybridoma Bank. We thank Carlos Espinoza, Sion Yang and Jeanine M. Ruggeri for technical supports. Special thanks to Daniel Long for prompt histopathology services. **Funding:** This work was supported by the Cancer Moonshot Initiative (U01CA-224145) to MPM and HCC. This project was also supported by NIH/NCI grants R01CA151588, R01CA198074, the University of Michigan Cancer Center Support Grant (NCI P30CA046592), the American Cancer Society to MPM and NCI-R50CA232985 to YZ. This project was also supported by 3-P30-CA-046592-28-S2 (Administrative Supplement to the Cancer Center Core Grant) to HCC and MPdM. FB was funded by the Association of Academic Surgery Joel Roslyn Award. TLF was funded by K08CA201581. NS is a recipient of the American Cancer Society Postdoctoral Award. ZCN was supported by Michigan Postdoctoral Pioneer Program, University of Michigan Medical School. RM was supported by T-32-GM007315; SBK was supported by T32-GM113900; NS, CJH, VS and KD were supported by T32-CA009676. AVD was supported by Rackham Merit Fellowship Program. The funders had no role in study design, data collection and analysis, decision to publish, or preparation of the manuscript. This work was made possible by the Tissue and Molecular Pathology and the Flow Cytometry Shared resources at the Rogel Cancer Center and the University of Michigan DNA Sequencing Core. CyTOF samples were run at the University of Rochester Medical Center Flow Cytometry Shared Resource and at the Indiana University Simon Cancer Center Flow Cytometry service.

References

1. Siegel RL, Miller KD, Jemal A. Cancer statistics, 2018. *CA Cancer J Clin* 2018;68(1):7–30 doi 10.3322/caac.21442. [PubMed: 29313949]
2. Vonderheide RH. The Immune Revolution: A Case for Priming, Not Checkpoint. *Cancer Cell* 2018;33(4):563–9 doi 10.1016/j.ccell.2018.03.008. [PubMed: 29634944]

3. Brahmer JR, Tykodi SS, Chow LQ, Hwu WJ, Topalian SL, Hwu P, et al. Safety and activity of anti-PD-L1 antibody in patients with advanced cancer. *N Engl J Med* 2012;366(26):2455–65 doi 10.1056/NEJMoa1200694. [PubMed: 22658128]
4. Hezel AF, Kimmelman AC, Stanger BZ, Bardeesy N, Depinho RA. Genetics and biology of pancreatic ductal adenocarcinoma. *Genes Dev* 2006;20(10):1218–49 doi 10.1101/gad.1415606. [PubMed: 16702400]
5. Ying H, Dey P, Yao W, Kimmelman AC, Draetta GF, Maitra A, et al. Genetics and biology of pancreatic ductal adenocarcinoma. *Genes Dev* 2016;30(4):355–85 doi 10.1101/gad.275776.115. [PubMed: 26883357]
6. Witkiewicz AK, McMillan EA, Balaji U, Baek G, Lin WC, Mansour J, et al. Whole-exome sequencing of pancreatic cancer defines genetic diversity and therapeutic targets. *Nat Commun* 2015;6:6744 doi 10.1038/ncomms7744. [PubMed: 25855536]
7. Kanda M, Matthaei H, Wu J, Hong SM, Yu J, Borges M, et al. Presence of somatic mutations in most early-stage pancreatic intraepithelial neoplasia. *Gastroenterology* 2012;142(4):730–3 e9 doi 10.1053/j.gastro.2011.12.042. [PubMed: 22226782]
8. Hingorani SR, Petricoin EF, Maitra A, Rajapakse V, King C, Jacobetz MA, et al. Preinvasive and invasive ductal pancreatic cancer and its early detection in the mouse. *Cancer Cell* 2003;4(6):437–50. [PubMed: 14706336]
9. Aguirre AJ, Bardeesy N, Sinha M, Lopez L, Tuveson DA, Horner J, et al. Activated Kras and Ink4a/Arf deficiency cooperate to produce metastatic pancreatic ductal adenocarcinoma. *Genes Dev* 2003;17(24):3112–26 doi 10.1101/gad.1158703. [PubMed: 14681207]
10. Clark CE, Hingorani SR, Mick R, Combs C, Tuveson DA, Vonderheide RH. Dynamics of the immune reaction to pancreatic cancer from inception to invasion. *Cancer Res* 2007;67(19):9518–27 doi 10.1158/0008-5472.CAN-07-0175. [pii] [PubMed: 17909062]
11. Stromnes IM, Brockenbrough JS, Izeradjene K, Carlson MA, Cuevas C, Simmons RM, et al. Targeted depletion of an MDSC subset unmasks pancreatic ductal adenocarcinoma to adaptive immunity. *Gut* 2014;63(11):1769–81 doi 10.1136/gutjnl-2013-306271. [PubMed: 24555999]
12. Mitchem JB, Brennan DJ, Knolhoff BL, Belt BA, Zhu Y, Sanford DE, et al. Targeting tumor-infiltrating macrophages decreases tumor-initiating cells, relieves immunosuppression, and improves chemotherapeutic responses. *Cancer Res* 2013;73(3):1128–41 doi 10.1158/0008-5472.CAN-12-27310008-5472.CAN-12-2731 [pii]. [PubMed: 23221383]
13. Zhu Y, Knolhoff BL, Meyer MA, Nywening TM, West BL, Luo J, et al. CSF1/CSF1R blockade reprograms tumor-infiltrating macrophages and improves response to T-cell checkpoint immunotherapy in pancreatic cancer models. *Cancer Res* 2014;74(18):5057–69 doi 10.1158/0008-5472.CAN-13-3723. [PubMed: 25082815]
14. Griesmann H, Drexel C, Milosevic N, Sipos B, Rosendahl J, Gress TM, et al. Pharmacological macrophage inhibition decreases metastasis formation in a genetic model of pancreatic cancer. *Gut* 2017;66(7):1278–85 doi 10.1136/gutjnl-2015-310049. [PubMed: 27013602]
15. Di Caro G, Cortese N, Castino GF, Grizzi F, Gavazzi F, Ridolfi C, et al. Dual prognostic significance of tumour-associated macrophages in human pancreatic adenocarcinoma treated or untreated with chemotherapy. *Gut* 2016;65(10):1710–20 doi 10.1136/gutjnl-2015-309193. [PubMed: 26156960]
16. Liou GY, Doppler H, Necela B, Edenfield B, Zhang L, Dawson DW, et al. Mutant KRAS-induced expression of ICAM-1 in pancreatic acinar cells causes attraction of macrophages to expedite the formation of precancerous lesions. *Cancer Discov* 2015;5(1):52–63 doi 10.1158/2159-8290.CD-14-0474 2159–8290.CD-14-0474 [pii]. [PubMed: 25361845]
17. Zhang Y, Yan W, Mathew E, Bednar F, Wan S, Collins MA, et al. CD4+ T lymphocyte ablation prevents pancreatic carcinogenesis in mice. *Cancer Immunol Res* 2014;2(5):423–35 doi 10.1158/2326-6066.CIR-14-0016-T 2326–6066.CIR-14-0016-T [pii]. [PubMed: 24795355]
18. Zhang Y, Velez-Delgado A, Mathew E, Li D, Mendez FM, Flannagan K, et al. Myeloid cells are required for PD-1/PD-L1 checkpoint activation and the establishment of an immunosuppressive environment in pancreatic cancer. *Gut* 2017;66(1):124–36 doi 10.1136/gutjnl-2016-312078. [PubMed: 27402485]

19. Daley D, Zambirinis CP, Seifert L, Akkad N, Mohan N, Werba G, et al. gammadelta T Cells Support Pancreatic Oncogenesis by Restraining alphabeta T Cell Activation. *Cell* 2016;166(6):1485–99 e15 doi 10.1016/j.cell.2016.07.046. [PubMed: 27569912]
20. Winograd R, Byrne KT, Evans RA, Odorizzi PM, Meyer AR, Bajor DL, et al. Induction of T-cell Immunity Overcomes Complete Resistance to PD-1 and CTLA-4 Blockade and Improves Survival in Pancreatic Carcinoma. *Cancer Immunol Res* 2015;3(4):399–411 doi 10.1158/2326-6066.CIR-14-0215. [PubMed: 25678581]
21. Jang JE, Hajdu CH, Liot C, Miller G, Dustin ML, Bar-Sagi D. Crosstalk between Regulatory T Cells and Tumor-Associated Dendritic Cells Negates Anti-tumor Immunity in Pancreatic Cancer. *Cell Rep* 2017;20(3):558–71 doi 10.1016/j.celrep.2017.06.062. [PubMed: 28723561]
22. Gunderson AJ, Kaneda MM, Tsujikawa T, Nguyen AV, Affara NI, Ruffell B, et al. Bruton Tyrosine Kinase-Dependent Immune Cell Cross-talk Drives Pancreas Cancer. *Cancer Discov* 2016;6(3):270–85 doi 10.1158/2159-8290.CD-15-0827. [PubMed: 26715645]
23. McAllister F, Bailey JM, Alsina J, Nirschl CJ, Sharma R, Fan H, et al. Oncogenic Kras activates a hematopoietic-to-epithelial IL-17 signaling axis in preinvasive pancreatic neoplasia. *Cancer Cell* 2014;25(5):621–37 doi 10.1016/j.ccr.2014.03.014S1535-6108(14)00122-6 [pii]. [PubMed: 24823639]
24. Balachandran VP, Luksza M, Zhao JN, Makarov V, Moral JA, Remark R, et al. Identification of unique neoantigen qualities in long-term survivors of pancreatic cancer. *Nature* 2017;551(7681):512–6 doi 10.1038/nature24462. [PubMed: 29132146]
25. Liyanage UK, Moore TT, Joo HG, Tanaka Y, Herrmann V, Doherty G, et al. Prevalence of regulatory T cells is increased in peripheral blood and tumor microenvironment of patients with pancreas or breast adenocarcinoma. *J Immunol* 2002;169(5):2756–61 doi 10.4049/jimmunol.169.5.2756. [PubMed: 12193750]
26. Hiraoka N, Onozato K, Kosuge T, Hirohashi S. Prevalence of FOXP3+ regulatory T cells increases during the progression of pancreatic ductal adenocarcinoma and its premalignant lesions. *Clin Cancer Res* 2006;12(18):5423–34 doi 10.1158/1078-0432.CCR-06-0369 [pii]. [PubMed: 17000676]
27. Tang Y, Xu X, Guo S, Zhang C, Tian Y, Ni B, et al. An increased abundance of tumor-infiltrating regulatory T cells is correlated with the progression and prognosis of pancreatic ductal adenocarcinoma. *PLoS One* 2014;9(3):e91551 doi 10.1371/journal.pone.0091551 PONE-D-13-42001 [pii]. [PubMed: 24637664]
28. Amir el AD, Davis KL, Tadmor MD, Simonds EF, Levine JH, Bendall SC, et al. viSNE enables visualization of high dimensional single-cell data and reveals phenotypic heterogeneity of leukemia. *Nat Biotechnol* 2013;31(6):545–52 doi 10.1038/nbt.2594. [PubMed: 23685480]
29. Van Gassen S, Callebaut B, Van Helden MJ, Lambrecht BN, Demeester P, Dhaene T, et al. FlowSOM: Using self-organizing maps for visualization and interpretation of cytometry data. *Cytometry A* 2015;87(7):636–45 doi 10.1002/cyto.a.22625. [PubMed: 25573116]
30. Lazarus J, Maj T, Smith JJ, Perusina Lanfranca M, Rao A, D'Angelica MI, et al. Spatial and phenotypic immune profiling of metastatic colon cancer. *JCI Insight* 2018;3(22) doi 10.1172/jci.insight.121932.
31. Collins MA, Bednar F, Zhang Y, Brisset JC, Galban S, Galban CJ, et al. Oncogenic Kras is required for both the initiation and maintenance of pancreatic cancer in mice. *J Clin Invest* 2012;122(2):639–53 doi 10.1172/JCI5922759227 [pii]. [PubMed: 22232209]
32. Collins MA, Brisset JC, Zhang Y, Bednar F, Pierre J, Heist KA, et al. Metastatic pancreatic cancer is dependent on oncogenic Kras in mice. *PLoS One* 2012;7(12):e49707 doi 10.1371/journal.pone.0049707PONE-D-12-09212 [pii]. [PubMed: 23226501]
33. Sakaguchi S, Miyara M, Costantino CM, Hafler DA. FOXP3+ regulatory T cells in the human immune system. *Nat Rev Immunol* 2010;10(7):490–500 doi 10.1038/nri2785. [PubMed: 20559327]
34. Kim JM, Rasmussen JP, Rudensky AY. Regulatory T cells prevent catastrophic autoimmunity throughout the lifespan of mice. *Nat Immunol* 2007;8(2):191–7 doi 10.1038/ni1428. [PubMed: 17136045]

35. Guerra C, Schuhmacher AJ, Canamero M, Grippo PJ, Verdaguer L, Perez-Gallego L, et al. Chronic pancreatitis is essential for induction of pancreatic ductal adenocarcinoma by K-Ras oncogenes in adult mice. *Cancer Cell* 2007;11(3):291–302 doi 10.1016/j.ccr.2007.01.012. [PubMed: 17349585]
36. Carriere C, Young AL, Gunn JR, Longnecker DS, Korc M. Acute pancreatitis markedly accelerates pancreatic cancer progression in mice expressing oncogenic Kras. *Biochem Biophys Res Commun* 2009;382(3):561–5 doi 10.1016/j.bbrc.2009.03.068. [PubMed: 19292977]
37. Morris JPt, Wang SC, Hebrok M. KRAS, Hedgehog, Wnt and the twisted developmental biology of pancreatic ductal adenocarcinoma. *Nat Rev Cancer* 2010;10(10):683–95 doi 10.1038/nrc2899. [PubMed: 20814421]
38. Ardito CM, Gruner BM, Takeuchi KK, Lubeseder-Martellato C, Teichmann N, Mazur PK, et al. EGF receptor is required for KRAS-induced pancreatic tumorigenesis. *Cancer Cell* 2012;22(3):304–17 doi 10.1016/j.ccr.2012.07.024S1535-6108(12)00337-6 [pii]. [PubMed: 22975374]
39. Guerra C, Collado M, Navas C, Schuhmacher AJ, Hernandez-Porras I, Canamero M, et al. Pancreatitis-induced inflammation contributes to pancreatic cancer by inhibiting oncogene-induced senescence. *Cancer Cell* 2011;19(6):728–39 doi 10.1016/j.ccr.2011.05.011. [PubMed: 21665147]
40. Morris JPt, Cano DA, Sekine S, Wang SC, Hebrok M. Beta-catenin blocks Kras-dependent reprogramming of acini into pancreatic cancer precursor lesions in mice. *J Clin Invest* 2010;120(2):508–20 doi 10.1172/JCI40045. [PubMed: 20071774]
41. Biffi G, Oni TE, Spielman B, Hao Y, Elyada E, Park Y, et al. IL1-Induced JAK/STAT Signaling Is Antagonized by TGFbeta to Shape CAF Heterogeneity in Pancreatic Ductal Adenocarcinoma. *Cancer Discov* 2019;9(2):282–301 doi 10.1158/2159-8290.CD-18-0710. [PubMed: 30366930]
42. Ohlund D, Handly-Santana A, Biffi G, Elyada E, Almeida AS, Ponz-Sarvise M, et al. Distinct populations of inflammatory fibroblasts and myofibroblasts in pancreatic cancer. *J Exp Med* 2017;214(3):579–96 doi 10.1084/jem.20162024. [PubMed: 28232471]
43. Rodriguez PC, Quiceno DG, Zabaleta J, Ortiz B, Zea AH, Piazuolo MB, et al. Arginase I production in the tumor microenvironment by mature myeloid cells inhibits T-cell receptor expression and antigen-specific T-cell responses. *Cancer Res* 2004;64(16):5839–49 doi 10.1158/0008-5472.CAN-04-0465. [PubMed: 15313928]
44. Geiger R, Rieckmann JC, Wolf T, Basso C, Feng Y, Fuhrer T, et al. L-Arginine Modulates T Cell Metabolism and Enhances Survival and Anti-tumor Activity. *Cell* 2016;167(3):829–42 e13 doi 10.1016/j.cell.2016.09.031. [PubMed: 27745970]
45. Hingorani SR, Wang L, Multani AS, Combs C, Deramandt TB, Hruban RH, et al. Trp53R172H and KrasG12D cooperate to promote chromosomal instability and widely metastatic pancreatic ductal adenocarcinoma in mice. *Cancer Cell* 2005;7(5):469–83. [PubMed: 15894267]
46. Long KB, Gladney WL, Tooker GM, Graham K, Fraietta JA, Beatty GL. IFNgamma and CCL2 Cooperate to Redirect Tumor-Infiltrating Monocytes to Degrade Fibrosis and Enhance Chemotherapy Efficacy in Pancreatic Carcinoma. *Cancer Discov* 2016;6(4):400–13 doi 10.1158/2159-8290.CD-15-1032. [PubMed: 26896096]
47. Griffith JW, Sokol CL, Luster AD. Chemokines and chemokine receptors: positioning cells for host defense and immunity. *Annu Rev Immunol* 2014;32:659–702 doi 10.1146/annurev-immunol-032713-120145. [PubMed: 24655300]
48. Elyada E, Bolisetty M, Laise P, Flynn WF, Courtois ET, Burkhart RA, et al. Cross-Species Single-Cell Analysis of Pancreatic Ductal Adenocarcinoma Reveals Antigen-Presenting Cancer-Associated Fibroblasts. *Cancer Discov* 2019;9(8):1102–23 doi 10.1158/2159-8290.CD-19-0094. [PubMed: 31197017]
49. Ochi A, Nguyen AH, Bedrosian AS, Mushlin HM, Zerbakhsh S, Barilla R, et al. MyD88 inhibition amplifies dendritic cell capacity to promote pancreatic carcinogenesis via Th2 cells. *J Exp Med* 2012;209(9):1671–87 doi 10.1084/jem.20111706. [PubMed: 22908323]
50. De Monte L, Reni M, Tassi E, Clavenna D, Papa I, Recalde H, et al. Intratumor T helper type 2 cell infiltrate correlates with cancer-associated fibroblast thymic stromal lymphopoietin production and reduced survival in pancreatic cancer. *J Exp Med* 2011;208(3):469–78 doi 10.1084/jem.20101876. [PubMed: 21339327]

51. Evans RA, Diamond MS, Rech AJ, Chao T, Richardson MW, Lin JH, et al. Lack of immunoediting in murine pancreatic cancer reversed with neoantigen. *JCI Insight* 2016;1(14) doi 10.1172/jci.insight.88328.
52. Shabaneh TB, Molodtsov AK, Steinberg SM, Zhang P, Torres GM, Mohamed GA, et al. Oncogenic BRAF(V600E) Governs Regulatory T-cell Recruitment during Melanoma Tumorigenesis. *Cancer Res* 2018;78(17):5038–49 doi 10.1158/0008-5472.CAN-18-0365. [PubMed: 30026331]
53. Feig C, Jones JO, Kraman M, Wells RJ, Deonaraine A, Chan DS, et al. Targeting CXCL12 from FAP-expressing carcinoma-associated fibroblasts synergizes with anti-PD-L1 immunotherapy in pancreatic cancer. *Proc Natl Acad Sci U S A* 2013;110(50):20212–7 doi 10.1073/pnas.1320318110. [PubMed: 24277834]
54. Ozdemir BC, Pentcheva-Hoang T, Carstens JL, Zheng X, Wu CC, Simpson TR, et al. Depletion of carcinoma-associated fibroblasts and fibrosis induces immunosuppression and accelerates pancreas cancer with reduced survival. *Cancer Cell* 2014;25(6):719–34 doi 10.1016/j.ccr.2014.04.005. [PubMed: 24856586]
55. Ijichi H, Chytil A, Gorska AE, Aakre ME, Fujitani Y, Fujitani S, et al. Aggressive pancreatic ductal adenocarcinoma in mice caused by pancreas-specific blockade of transforming growth factor-beta signaling in cooperation with active Kras expression. *Genes Dev* 2006;20(22):3147–60 doi 10.1101/gad.1475506. [PubMed: 17114585]
56. Sherman MH, Yu RT, Engle DD, Ding N, Atkins AR, Tiriach H, et al. Vitamin D receptor-mediated stromal reprogramming suppresses pancreatitis and enhances pancreatic cancer therapy. *Cell* 2014;159(1):80–93 doi 10.1016/j.cell.2014.08.007. [PubMed: 25259922]
57. Jiang H, Hegde S, Knolhoff BL, Zhu Y, Herndon JM, Meyer MA, et al. Targeting focal adhesion kinase renders pancreatic cancers responsive to checkpoint immunotherapy. *Nat Med* 2016;22(8):851–60 doi 10.1038/nm.4123. [PubMed: 27376576]
58. Provenzano PP, Cuevas C, Chang AE, Goel VK, Von Hoff DD, Hingorani SR. Enzymatic targeting of the stroma ablates physical barriers to treatment of pancreatic ductal adenocarcinoma. *Cancer Cell* 2012;21(3):418–29 doi 10.1016/j.ccr.2012.01.007. [PubMed: 22439937]
59. Jacobetz MA, Chan DS, Nesses A, Bapiro TE, Cook N, Frese KK, et al. Hyaluronan impairs vascular function and drug delivery in a mouse model of pancreatic cancer. *Gut* 2013;62(1):112–20 doi 10.1136/gutjnl-2012-302529. [PubMed: 22466618]
60. Alexeev V, Donahue A, Uitto J, Igoucheva O. Chemotaxis-driven disease-site targeting of therapeutic adult stem cells in dystrophic epidermolysis bullosa. *Stem Cell Res Ther* 2016;7(1):124 doi 10.1186/s13287-016-0388-y. [PubMed: 27568180]
61. Lebre MC, Vergunst CE, Choi IY, Aarrass S, Oliveira AS, Wyant T, et al. Why CCR2 and CCR5 blockade failed and why CCR1 blockade might still be effective in the treatment of rheumatoid arthritis. *PLoS One* 2011;6(7):e21772 doi 10.1371/journal.pone.0021772. [PubMed: 21747955]
62. Dairaghi DJ, Oyajobi BO, Gupta A, McCluskey B, Miao S, Powers JP, et al. CCR1 blockade reduces tumor burden and osteolysis in vivo in a mouse model of myeloma bone disease. *Blood* 2012;120(7):1449–57 doi 10.1182/blood-2011-10-384784. [PubMed: 22618707]
63. Kitamura T, Fujishita T, Loetscher P, Revesz L, Hashida H, Kizaka-Kondoh S, et al. Inactivation of chemokine (C-C motif) receptor 1 (CCR1) suppresses colon cancer liver metastasis by blocking accumulation of immature myeloid cells in a mouse model. *Proc Natl Acad Sci U S A* 2010;107(29):13063–8 doi 10.1073/pnas.1002372107. [PubMed: 20616008]
64. Barilla RM, Diskin B, Caso RC, Lee KB, Mohan N, Buttar C, et al. Specialized dendritic cells induce tumor-promoting IL-10(+)IL-17(+) FoxP3(neg) regulatory CD4(+) T cells in pancreatic carcinoma. *Nat Commun* 2019;10(1):1424 doi 10.1038/s41467-019-09416-2. [PubMed: 30926808]
65. Sanford DE, Belt BA, Panni RZ, Mayer A, Deshpande AD, Carpenter D, et al. Inflammatory monocyte mobilization decreases patient survival in pancreatic cancer: a role for targeting the CCL2/CCR2 axis. *Clin Cancer Res* 2013;19(13):3404–15 doi 10.1158/1078-0432.CCR-13-0525. [PubMed: 23653148]
66. Nywening TM, Wang-Gillam A, Sanford DE, Belt BA, Panni RZ, Cusworth BM, et al. Targeting tumour-associated macrophages with CCR2 inhibition in combination with FOLFIRINOX in patients with borderline resectable and locally advanced pancreatic cancer: a single-centre, open-

- label, dose-finding, non-randomised, phase 1b trial. *Lancet Oncol* 2016;17(5):651–62 doi 10.1016/S1470-2045(16)00078-4. [PubMed: 27055731]
67. Nywening TM, Belt BA, Cullinan DR, Panni RZ, Han BJ, Sanford DE, et al. Targeting both tumour-associated CXCR2(+) neutrophils and CCR2(+) macrophages disrupts myeloid recruitment and improves chemotherapeutic responses in pancreatic ductal adenocarcinoma. *Gut* 2018;67(6):1112–23 doi 10.1136/gutjnl-2017-313738. [PubMed: 29196437]
68. Halbrook CJ, Pontious C, Kovalenko I, Lapienyte L, Dreyer S, Lee HJ, et al. Macrophage-Released Pyrimidines Inhibit Gemcitabine Therapy in Pancreatic Cancer. *Cell Metab* 2019;29(6):1390–9 e6 doi 10.1016/j.cmet.2019.02.001. [PubMed: 30827862]
69. Zhang Y, Morris JPt, Yan W, Schofield HK, Gurney A, Simeone DM, et al. Canonical wnt signaling is required for pancreatic carcinogenesis. *Cancer Res* 2013;73(15):4909–22 doi 10.1158/0008-5472.CAN-12-43840008-5472.CAN-12-4384 [pii]. [PubMed: 23761328]
70. Bertaux-Skeirik N, Wunderlich M, Teal E, Chakrabarti J, Biesiada J, Mahe M, et al. CD44 variant isoform 9 emerges in response to injury and contributes to the regeneration of the gastric epithelium. *J Pathol* 2017;242(4):463–75 doi 10.1002/path.4918. [PubMed: 28497484]
71. Hosein AN, Huang H, Wang Z, Parmar K, Du W, Huang J, et al. Cellular heterogeneity during mouse pancreatic ductal adenocarcinoma progression at single-cell resolution. *JCI Insight* 2019 doi 10.1172/jci.insight.129212.

Significance

Here, we describe an unexpected crosstalk between Tregs and fibroblasts in pancreatic cancer. Treg depletion resulted in differentiation of inflammatory fibroblast subsets, in turn driving infiltration of myeloid cells through CCR1, thus uncovering a potentially new therapeutic approach to relieve immunosuppression in pancreatic cancer.

Author Manuscript

Author Manuscript

Author Manuscript

Author Manuscript

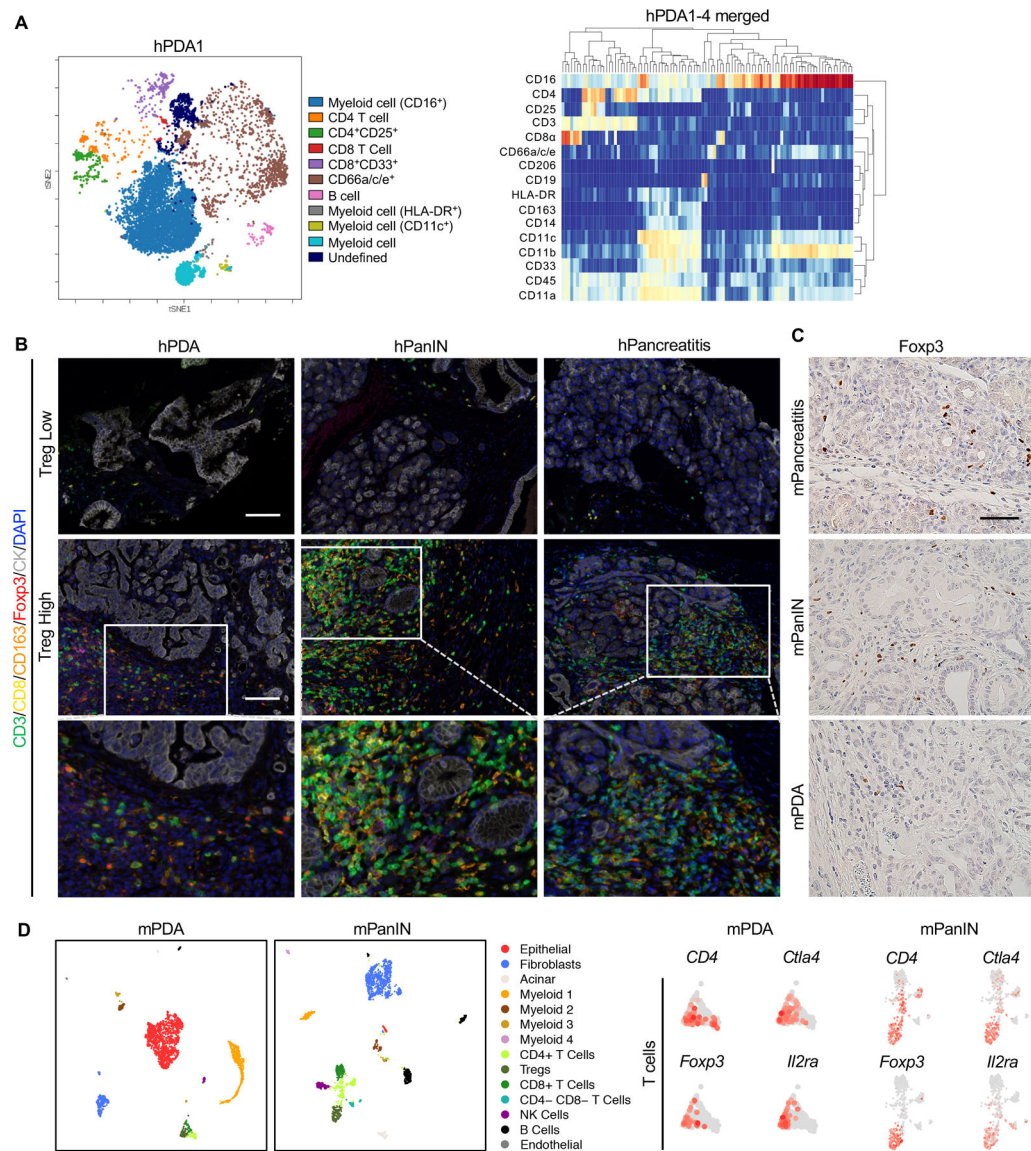


Figure 1. Regulatory T cells are prevalent in human PDA and PanINs.

(A) CyTOF immune profiling by FlowSOM-viSNE of human pancreatic tumors

demonstrating the presence of CD4⁺CD25⁺ Tregs. (B) Representative images of Opal

staining on human pancreatic lesion samples. Scale bar 100 μm. (C) Immunohistochemistry

staining for Foxp3 staining in mouse pancreatic tissues. Scale bar 50 μm. (D) UMAP plots

of single cell RNA sequencing analysis with mouse orthotopic pancreatic cancer samples or

PanIN lesions, color-coded by their associated cluster (left) or color-coded for expression

(gray to red) of *Cd4*, *Ctla4*, *Foxp3* and *Il2ra*.

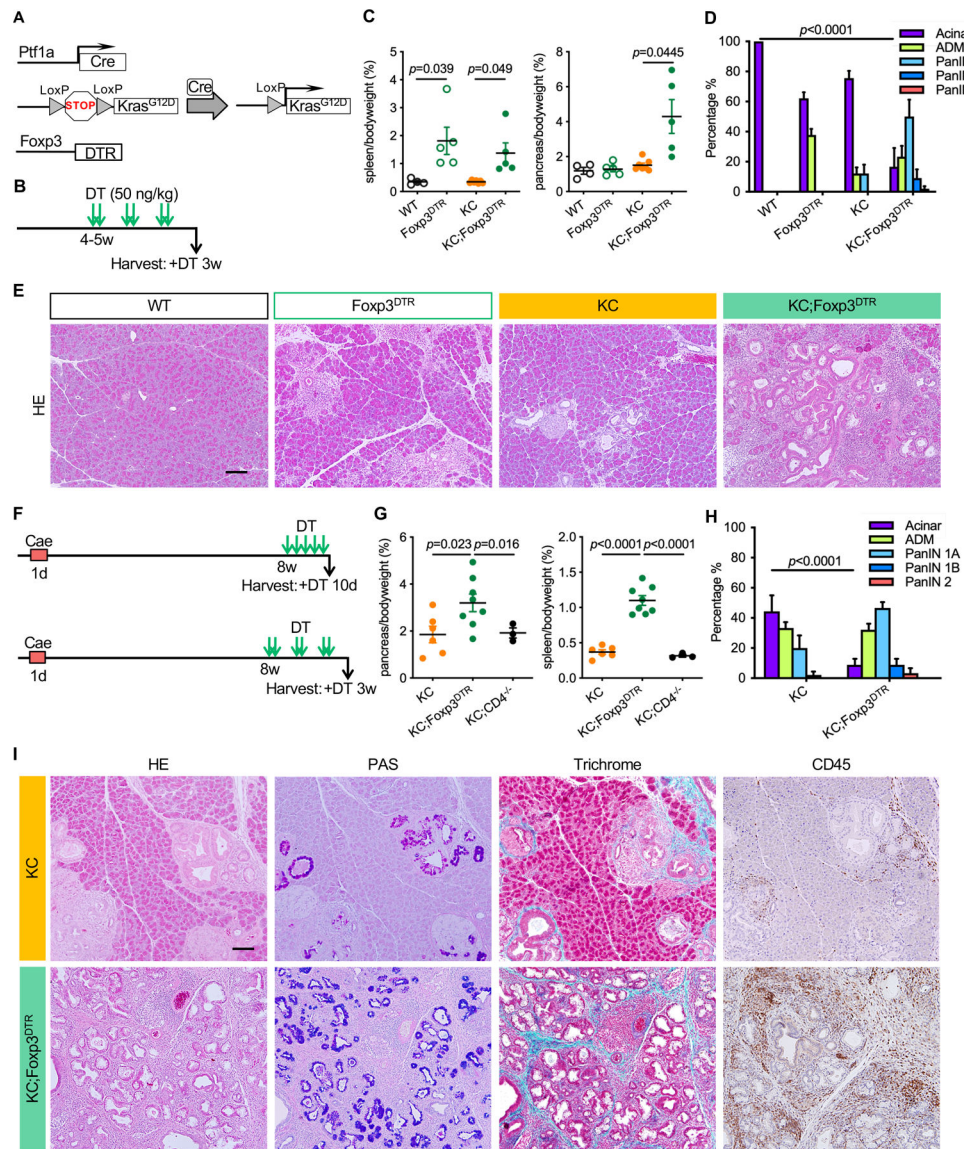


Figure 2. Treg depletion results in pancreatitis and promotes PanIN formation and progression. (A) Genetic makeup of the KC;Foxp3^{DTR} mouse model. (B) Experimental design, n=4–7mice/cohort. (C) Pancreas to body weight ratio and spleen to body weight ratio of WT, Foxp3^{DTR}, KC and KC;Foxp3^{DTR} mice after 3 weeks of DT treatment. Data represent mean ± SEM, n=4–7mice/cohort. The statistical difference was determined by two-tailed t-tests. (D) Histopathologic quantification of WT, Foxp3^{DTR}, KC and KC;Foxp3^{DTR} mice after 3 weeks of DT treatment. Data represent mean ± SEM, n = 3–4 mice/cohort. The statistical difference was determined by two-way ANOVA. (E) H&E staining of WT, Foxp3^{DTR}, KC and KC;Foxp3^{DTR} pancreata after 3 weeks of DT treatment. Scale bar 100 μm. (F) Experimental design, n=3–8 mice/cohort. (G) Pancreas to body weight ratio and spleen to body weight ratio of KC, KC;Foxp3^{DTR} and KC;CD4^{-/-} mice that received 3 weeks of DT treatment starting 8 weeks post caerulein. Data represent mean ± SEM, n=3–8 mice/cohort. The statistical difference was determined by two-tailed t-tests. (H) Histopathologic

quantification of KC and KC;F_{oxp3}^{DTR} mice received 3 weeks of DT treatment starting 8 weeks post caerulein.. Data represent mean ± SEM, n=3–4mice/cohort. The statistical difference was determined by two-way ANOVA. **(I)** H&E staining, Periodic acid–Schiff (PAS) staining, Gomori trichrome staining and immunohistochemistry staining for CD45 in KC and KC;F_{oxp3}^{DTR} mice that received 3 weeks of DT treatment starting 8 weeks post caerulein. Scale bar 100 μm.

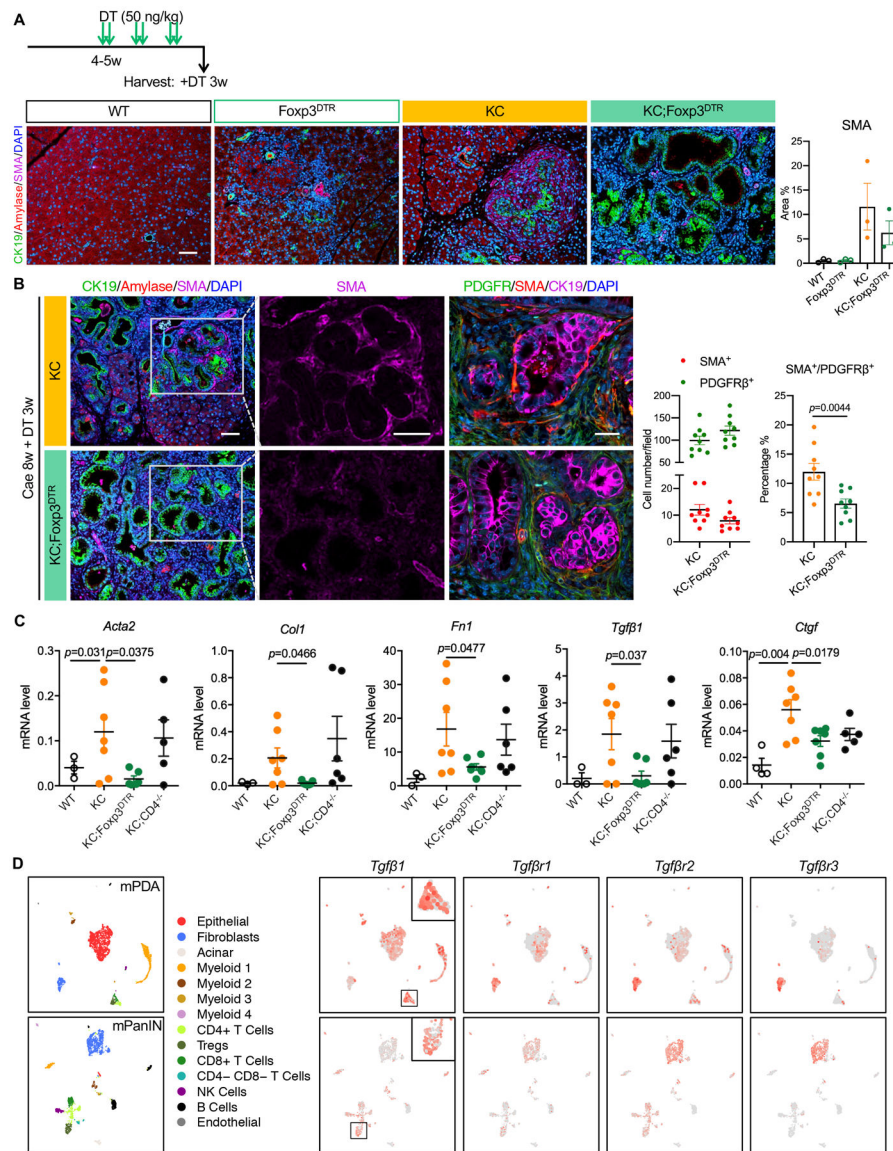


Figure 3. Treg depletion inactivates stromal fibroblasts.

(A) Experimental design (n=4–7 mice/cohort) and co-immunofluorescent staining for CK19 (green), Amylase (red), SMA (magenta) and DAPI (blue) in WT, Foxp3^{DTR}, KC and KC;Foxp3^{DTR} pancreata after 3 weeks of DT treatment. Scale bar 100 μ m. Quantification of SMA positive area is shown on the right. Data represent mean \pm SEM, n=3 slides/cohort. (B) co-immunofluorescent staining for CK19 (green), Amylase (red), SMA (magenta) and DAPI (blue). Scale bar 100 μ m. Quantification of SMA and PDGFR β positive cells is shown on the right. Data represent mean \pm SEM, n=9 images/cohort. The statistical difference was determined by two-tailed t-tests. (C) qRT-PCR for *α -SMA (Acta2)*, *Coll*, *Fn1*, *Tgf β 1* and *Ctgf* expression in WT control, KC, KC;Foxp3^{DTR} and KC;CD4^{-/-} pancreata. Mice received DT treatment following 8 weeks post caerulein. Data represent mean \pm SEM, n = 3–7 mice/cohort. The statistical difference was determined by two-tailed t-tests. (D) UMAP plots of single cell RNA sequencing analysis with mouse orthotopic pancreatic cancer

samples or PanIN lesions, color-coded by their associated cluster (left) or color-coded for expression (gray to red) of *Tgfβ1*, *Tgfβr1*, *Tgfβr2* and *Tgfβr3*.

Author Manuscript

Author Manuscript

Author Manuscript

Author Manuscript

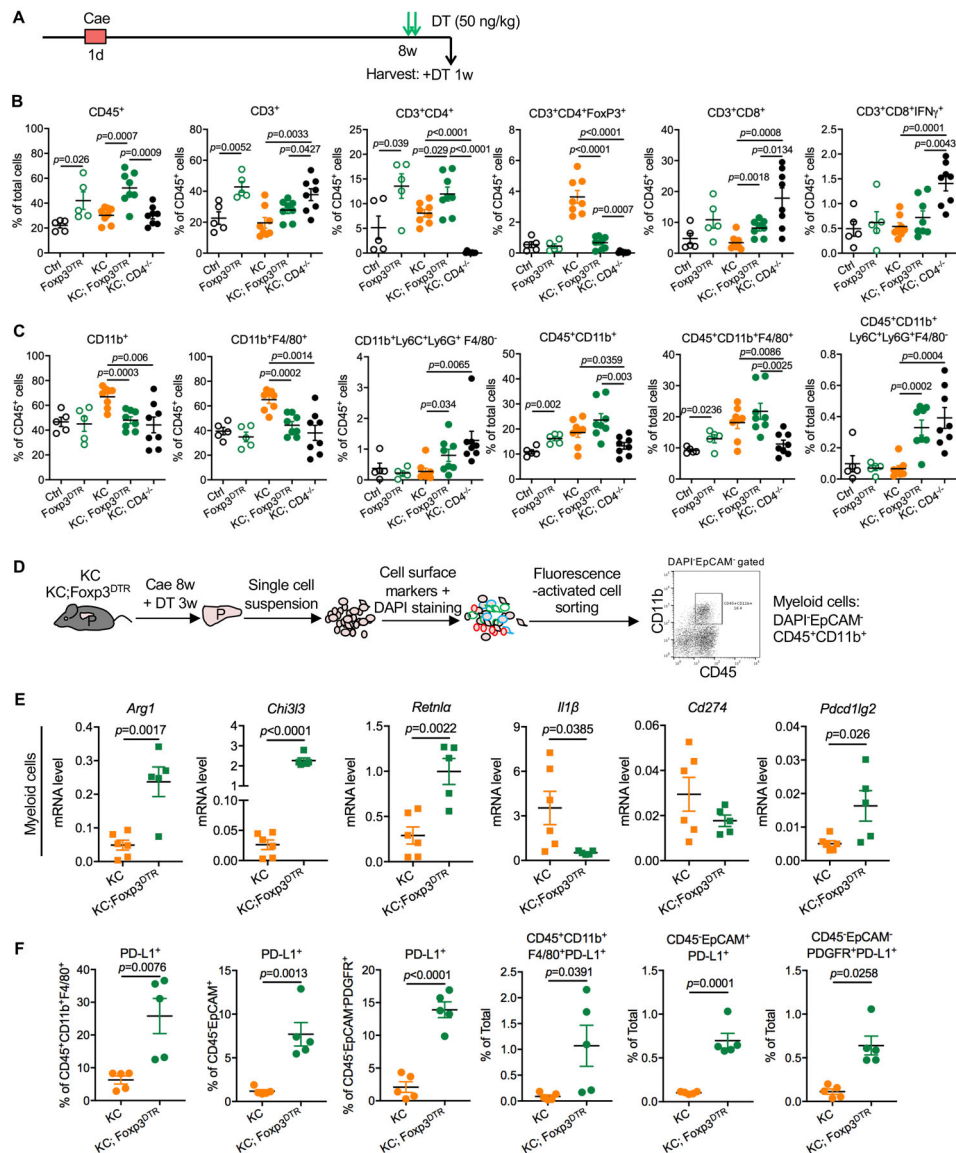


Figure 4. Characterization of pancreatic immune infiltrates.

(A) Experimental design, n=4–8 mice/cohort. (B) WT, Foxp3^{DTR}, KC, KC;Foxp3^{DTR} and KC;CD4^{-/-} mice received 1 week DT treatment following 8 weeks post pancreatitis induction. CD45⁺ leukocytes, CD3⁺ T cells, CD3⁺CD4⁺ T cells, CD3⁺CD4⁺FoxP3⁺ Tregs, CD3⁺CD8⁺ T cells, CD3⁺CD8⁺IFN γ ⁺ T cells and (C) CD11b⁺ myeloid cells, CD11b⁺F4/80⁺ macrophages and CD11b⁺Ly6C⁺Ly6G⁺F4/80⁺ MDSCs from pancreata were measured by flow cytometry as percentage of total cells or percentage of total leukocytes. Data represent mean \pm SEM, the statistical difference between experimental groups was determined by two-tailed t-tests. (D) Schematic illustration of pancreatic infiltrating myeloid cells extraction by fluorescence-activated cell sorting and a representative flow cytometry plot showing the gating strategy. (E) qRT-PCR for *Arg1*, *Chi3l3*, *Retnla*, *Il1 β* , *Cd274* and *Pdcd1lg2* expression in pancreatic myeloid cells derived from KC and KC;Foxp3^{DTR} mice that received 3-week DT treatment following 8 weeks post caerulein. Data represent mean

\pm SEM, n=5–6. The statistical difference was determined by two-tailed t-tests. **(F)** The percentage of PD-L1 expressing macrophages, epithelial cells and fibroblasts in KC and KC;Foxp3^{DTR} pancreata were measured by flow cytometry. Data represent mean \pm SEM, n=5. The statistical difference was determined by two-tailed t-tests.

Author Manuscript

Author Manuscript

Author Manuscript

Author Manuscript

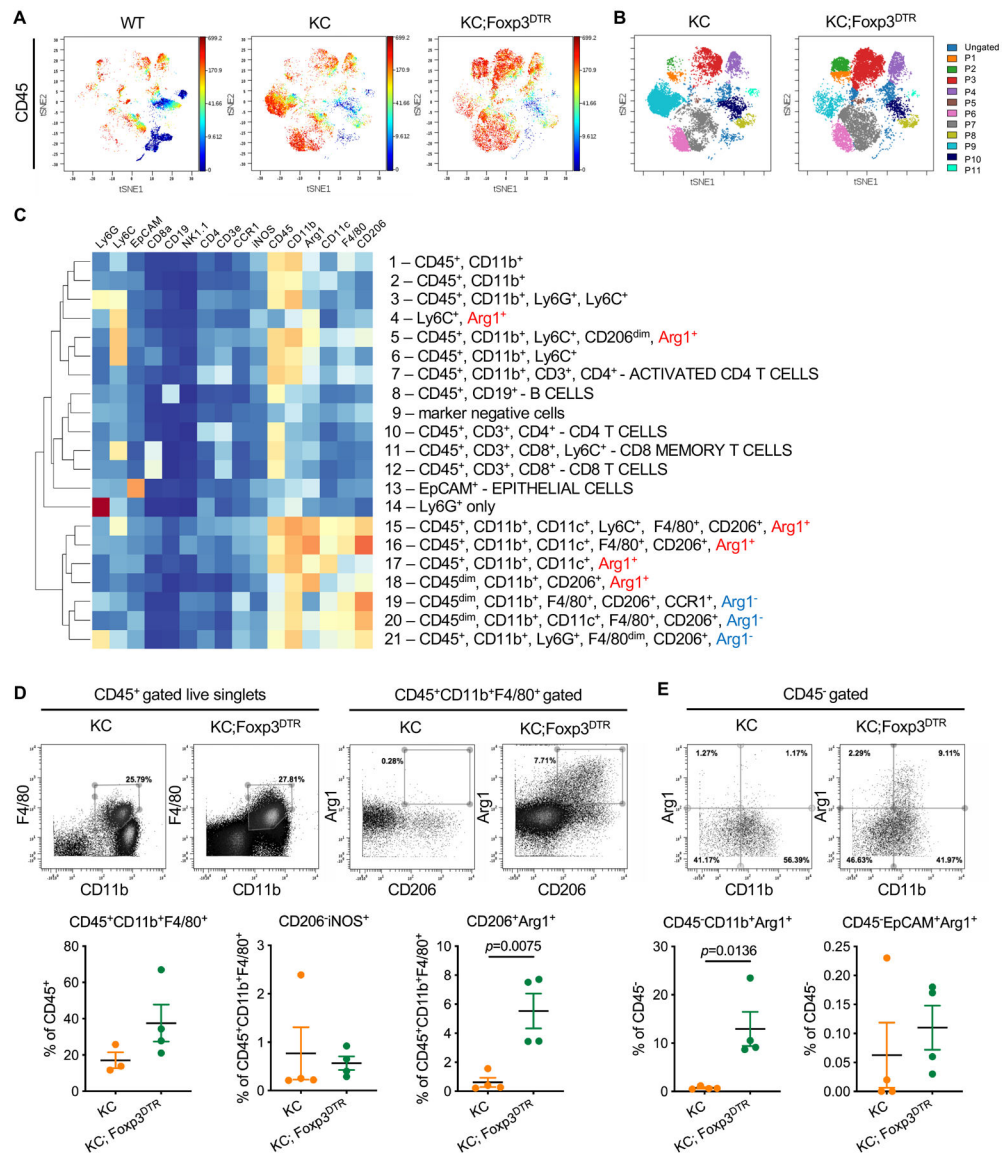


Figure 5. Tumor associated macrophages exhibit high immunosuppressive capacity upon Treg depletion.

(A) Representative viSNE plots (dot plots colored by CD45 channel) of WT, KC and KC;Foxp3^{DTR} pancreata that received 1-week DT treatment following 8 weeks post caerulein. (B) Immune cell populations identified by manual gating in viSNE maps, and (C) by supervised clustering of SPADE-identified subpopulations. (D) Top: representative CyTOF dot plots showing gating strategy defining tumor associated macrophages and CD206⁺Arg1⁺ M2-like macrophage subset. Bottom: quantification of the total macrophage and CD206⁻iNOS⁺ M1-like and CD206⁺Arg1⁺ M2-like macrophage subsets. (E) Representative CyTOF dot plots showing gating strategy defining CD11b⁺Arg1⁺ non-immune cell population, and quantification of the Arg1⁺ non-immune cell populations. Data represent mean±SEM, n=3–4. The statistical difference between KC and KC;Foxp3^{DTR} pancreata was determined by two-tailed t-tests.

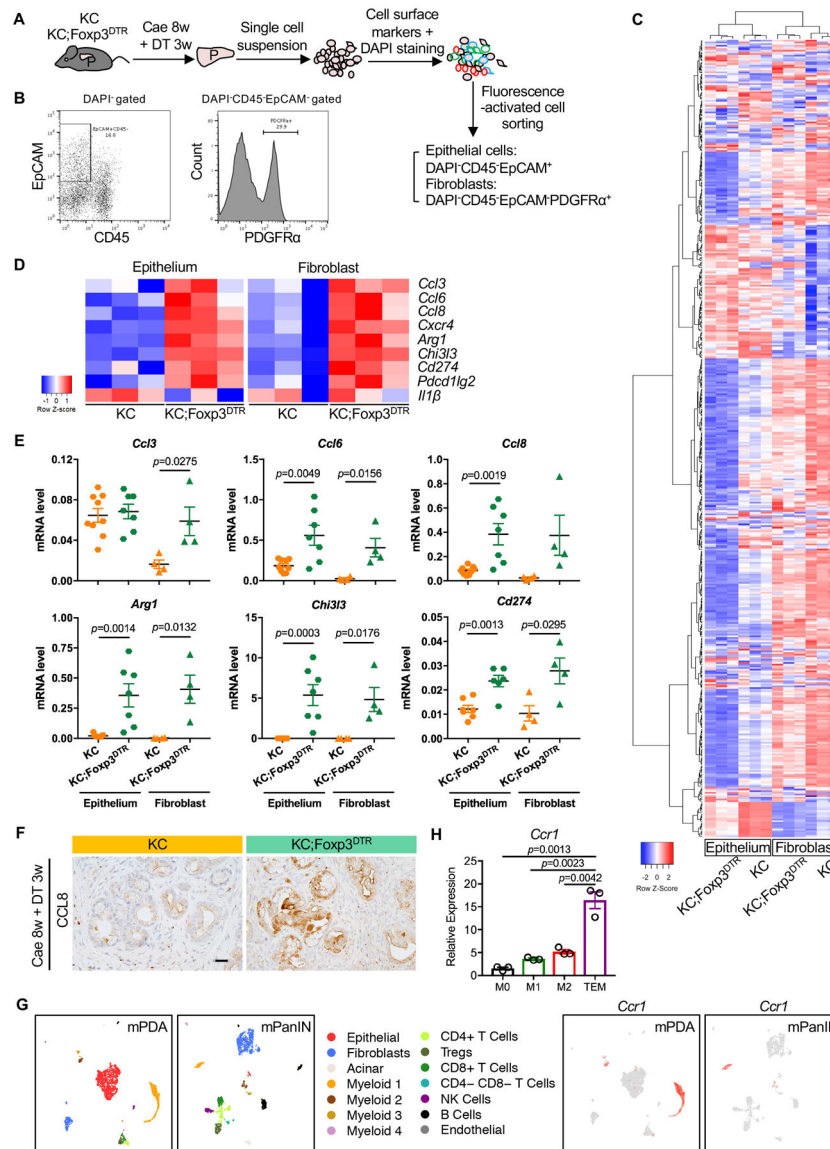


Figure 6. Gene expression profiling for pancreatic epithelial cells and fibroblasts upon Treg depletion.

(A) Schematic illustration of pancreatic epithelial cells and fibroblasts extraction by fluorescence-activated cell sorting. (B) Representative flow cytometry plots showing gating strategy to identify epithelial cells and fibroblasts. (C) Heat map showing differentially expressed secretome genes and (D) Top differentially expressed secretome genes in epithelial cells or fibroblasts between KC and KC;Foxp3^{DTR} pancreata. (E) qRT-PCR for *Ccl3*, *Ccl6*, *Ccl8*, *Arg1*, *Chi3l3* and *Cd274* expression in pancreatic epithelial cells or fibroblasts derived from KC and KC;Foxp3^{DTR} mice that received 3 weeks of DT treatment following 8 weeks post caerulein. Data represent mean \pm SEM, n=4–9. (F) Immunohistochemistry staining for CCL8 in KC and KC;Foxp3^{DTR} pancreata. Scale bar 50 μ m. (G) UMAP plots of single cell RNA sequencing analysis with mouse orthotopic pancreatic cancer samples or PanIN lesions, color-coded by their associated cluster (left) or color-coded for expression (gray to red) of *Ccr1*. (H) qRT-PCR for *Ccr1* expression in bone

marrow derived macrophages under different polarization status. Data represent mean \pm SEM, n=3. The statistical difference was determined by two-tailed t-tests.

Author Manuscript

Author Manuscript

Author Manuscript

Author Manuscript

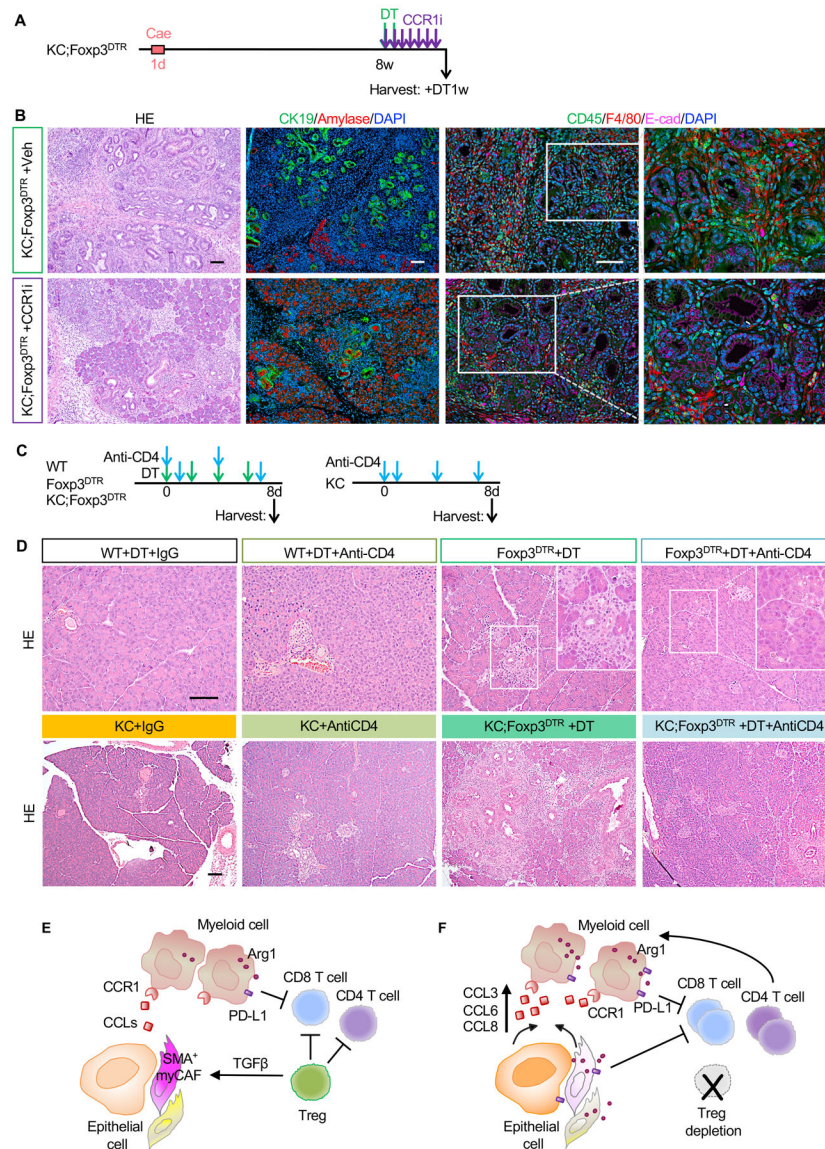


Figure 7. CCR1 inhibition and CD4⁺ T cell depletion abrogate Treg depletion induced PanIN progression.

(A) Experimental design, n=5–6 mice/cohort. (B) H&E staining, co-immunofluorescent staining for CK19 (green), Amylase (red) and DAPI (blue), and co-immunofluorescent staining for CD45 (green), F4/80 (red), E-cad (magenta) and DAPI (blue) in control and CCR1 inhibitor treated KC;Foxp3^{DTR} pancreata. Scale bar 100 μm. (C) Experimental design and (D) H&E staining for WT, Foxp3^{DTR}, KC and KC;Foxp3^{DTR} mice that received DT treatment and/or anti-CD4 antibody. n=3–4 mice/cohort. Scale bar 100 μm. (E) Working model. Tregs inhibit CD8⁺ T cells, but also restrain pathogenic CD4⁺ T cell responses. Tregs regulate the production of TGFβ thus promoting the differentiation of Smooth Muscle Actin (SMA)⁺ fibroblasts (myCAFs). (F) Treg depletion results in loss of TGFβ and compensatory changes in the fibroblast population that in turn secrete myeloid-recruiting chemokines, driving increased recruitment of myeloid cells and failing to alleviate immunosuppression.

Treg depletion also unleashes pathogenic CD4⁺ T cell responses that promote pancreatic inflammation and carcinogenesis.

Author Manuscript

Author Manuscript

Author Manuscript

Author Manuscript